The role of gamma oscillations in the modulation of memory consolidation by emotions

by

Vasiliki Kanta Chantzi

A dissertation submitted to the

Graduate School – Newark, Rutgers, The State University of New Jersey

in partial fulfillment of the requirements for the degree of

Doctor of Philosophy

Graduate Program in Behavioral and Neural Sciences

written under the direction of

Dr. Denis Paré

and approved by

_____

_____

_____

_____

_____

Newark, New Jersey

October, 2019

ABSTRACT OF THE DISSERTATION

The Role of Gamma Oscillations in the Modulation of Memory Consolidation by Emotions

By VASILIKI KANTA CHANTZI

Dissertation Director:

Dr. Denis Paré

Our everyday experiences, even for mundane events, can form long-lasting memories. While newly formed memories are labile at first, with time they may become permanent and resistant to forgetting. This process is called memory consolidation. For declarative memories, consolidation is thought to involve interactions between the neocortex and hippocampus during offline states such as sleep. Besides strengthening with time, memory consolidation is also influenced by emotional arousal. The facilitating effect of emotions on consolidation is mediated by the basolateral amygdala (BLA) and its strong projections to both the hippocampus and neocortex. In contrast to the extensive investigations of the electrophysiological mechanisms supporting systems consolidation between the hippocampus and neocortex, there has not been a comparable advancement in our understanding of the BLA's role. However, what is known is that the BLA generates robust gamma oscillations during emotional arousal, which can facilitate interregional interactions. In order to provide a unified understanding of memory consolidation, I examined how the consolidation of emotional experiences affects the interactions between the BLA, hippocampus and medial prefrontal cortex (mPFC), a neocortical area linked to

consolidation. In particular, I studied how gamma-related activity is affected after emotional learning. I then directly tested whether gamma oscillations in the BLA support consolidation, by using real-time optogenetic manipulation of these oscillations in the post-training consolidation period. My results show that gamma oscillations mediate the emotional facilitation of memory consolidation.

Acknowledgements

I would like to thank my advisor, Denis Pare, for his wonderful mentorship and support throughout my PhD. Denis helped me develop a scientific mind, taught me how to think about research and always fostered a caring lab environment. His advice and profound insight will be immensely valuable for the rest of my career. I would also like to express my deep gratitude to Drew Headley, who patiently shared with me his extensive knowledge on how to become a neurophysiologist, but most importantly a critical thinker. His guidance was fundamental throughout my thesis. I would also like to thank the members of my thesis committee: Dr. Pierre-Olivier Polack, Dr. Tibor Koos, Dr. Juan Mena-Segovia and Dr. Ryan LaLumiere, for devoting their time and helping me with their comments and suggestions. Many thanks to all current and past Pare lab members, for the support, insightful discussions and friendship throughout the years. I am also extremely grateful to my BNS friends for their constant encouragement and camaraderie. I will always cherish our common experiences and the time we spent together.

Special thanks to my amazing friends from Greece and New Jersey who were always there to help from day one. Finally, I am truly indebted to my family, especially my mother, Alexandra Hantzi, my late father, Aristotelis Kantas, as well as my husband, Peter Argyrakis, for their endless support and motivation, no matter the hardship. This thesis is dedicated to you.

Preface

All studies presented here are result of a collaboration between myself and Drew Headley. Chapters 4-7 are currently under consideration for publication. Chapter 3 is in preparation for publication.

Table of contents

List of figures

List of abbreviations

AAV: Adeno-associated vector

aCSF: Artificial cerebrospinal fluid

AMPA: Alpha-amino-3-hydroxy-5-methyl-4-isoxazolepropionic acid

ANOVA: Analysis of variance

AP: Anterioposterior

BLA: Basolateral amygdala

CA1: Cornu Ammonis 1

CA3: Cornu Ammonis 3

CeA: Central amygdala

CS: Conditioned stimulus

CSD: Current source density

CTC: Communication through coherence

dHipp: Dorsal hippocampus

DG: Dentate gyrus

DSs: Dentate spikes

DV: Dorsoventral

EEG: Electroencephalogram

EMG: Electromyogram

FPGA: Field programmable gate array

FS: Fast-spiking interneuron

GABA: Gamma-aminobutyric acid

$GABA_A$: Alpha class of gamma-aminobutyric acid receptors

HB: Holeboard task

HEPES: 4-(2-hydroxyethyl)-1-piperazineethanesulfonic acid

IA: Inhibitory avoidance

ING: Interneuron Network Gamma

ISI: Inter-light stimulus interval

LED: Light-emitting diode

LFP: Local field potential

LSD: Least significant difference

ML: Mediolateral

mPFC: Medial prefrontal cortex

MUA: Multiunit activity

NREM: Non-rapid eye movement

PBS: Phosphate-buffered saline

PING: Pyramidal Interneuron Network Gamma

PN: Principal neuron

PPC: Pairwise phase consistency

PSTH: Peri-stimulus time histograms

PTX: Picrotoxin

PV: Parvalbumin

SEM: Standard error of the mean

QW: Quiet waking

SD: Standard deviation

STR: Striatum

SWRs: Sharp-wave ripples

vHipp: Ventral hippocampus

CHAPTER 1

Introduction

When a new memory is first formed, it is vulnerable to interference from other experiences occurring closely in time. After this period of lability, some memories are stored for life. The mechanism through which memories are stabilized over time is called memory consolidation. In addition, emotionally arousing events are remembered more vividly than mundane experiences, indicating a relationship between the emotional content of an experience and subsequent memory strength. Both phenomena have been extensively studied, but mostly in isolation, rarely delving into their interactions. In this introduction, I will describe both processes and the links between them.

1.1 Memories stabilize slowly over time

As mentioned before, new memories undergo a period of susceptibility to outside influences, wherein they can be disrupted by exposure to new material (Mueller & Pilzecker, 1900). Furthermore, patients with selective medial temporal lobe lesions exhibit severe retrograde amnesia for recent declarative memories (Scoville & Milner, 1957), as

well as an inability to store new information (Squire & Alvarez, 1995). Memory formation is particularly susceptible to experimental disruption shortly after learning, such as by drugs or electrical stimulation (Cahill, 2000). This evidence suggested that memory consolidation is a process restricted in time that relies upon certain brain areas.

The two-stage model of memory consolidation

Early studies suggested that memory consolidation is a two-stage process, also called systems consolidation, with the hippocampus involved early on in the temporary storage of memories and the neocortex later becoming their permanent locus (Marr, 1970; Squire, 1986). In 1989, György Buzsáki proposed a specific two-stage neurophysiological model of systems consolidation (Buzsáki, 1989). In this model, new information is initially stored as labile traces in the hippocampus and neocortex. During this active state, weak intra- and interregional connections would be tagged by changes in neuronal excitability (Wiltgen et al., 2004). When the system goes offline during post-learning sleep, the same cells that were active during the experience would be reactivated and their connections strengthened. Through this process, the initially labile trace would be converted into a permanent memory (Born & Wilhelm, 2012). This ‘replay’ of experience-related activity patterns is thought to occur mostly in non-rapid eye movement (NREM) sleep, because it is a period of low sensory input, thus less susceptible to interference. In particular, ‘replay’ would occur during hippocampal population events named sharp wave ripples (SWRs). Therefore, successful memory consolidation in the two-stage model depends upon the reactivation of activity patterns by hippocampal SWRs during NREM sleep. Furthermore,

the hippocampus and neocortex play different roles in this model. I will now summarize how these phenomena participate in memory consolidation.

Key components for systems consolidation

Consistent with a pivotal role of NREM sleep in consolidation, boosting human cortical slow oscillations during post-learning NREM sleep by transcranial stimulation results in increased retention (Marshall et al., 2006; Ngo et al., 2013), while the same manipulation in rats results in long-term potentiation of cortical synapses (Chauvette et al., 2012) and enhancement of memory (Miyamoto et al., 2016). Together, these results suggest that post-learning NREM sleep facilitates the reactivation of experience-related ensembles and the strengthening of their connections, leading to successful consolidation.

During NREM sleep experience-related ensembles reactivate, a phenomenon known as 'replay' (Sutherland & McNaughton, 2000). To uncover experience-related activity during sleep, most studies use spatial tasks, since hippocampal cells fire at particular locations (hence the term 'place cells', O' Keefe, 1979), and thus their coordinated activity corresponds to locations in an environment. It was found that place cells activated during waking were preferentially active during subsequent NREM sleep (Pavlides & Winson, 1989). Furthermore, cell pairs that showed correlated firing during the spatial task also exhibited it in subsequent NREM sleep (Wilson & McNaughton, 1994). These correlations were enhanced during post-training SWRs (Kudrimoti et al., 1999), and not only are the same cells firing during SWRs, but they do so in the same order as during exploration, with spike sequences usually replayed on a compressed timescale

(Skaggs & McNaughton, 1996; Nádasdy et al., 1999). These nested patterns of activity first appear during quiet wakefulness, when the animal pauses between bouts of exploration (Jadhav et al., 2016; Wu et al., 2017; Drieu et al., 2018). Thus, neuronal activity reflecting recent experiences is re-instantiated during hippocampal SWRs in post-learning NREM sleep, which provides a critical mechanism for memory consolidation.

Irrespective of their precise relationship with replay, there is additional support for the importance of SWRs in memory consolidation. The incidence of SWRs is increased in the first sleep episode after associative learning (Eschenko et al., 2008; Ramadan et al., 2009), and is accompanied by enhanced hippocampal replay of waking activity (Kudrimoti et al., 1999). Furthermore, cells that are not active during learning show a gradual downregulation of synaptic strength during SWRs (Norimoto et al., 2018). Crucially, reducing SWR activity during post-training sleep impairs subsequent memory (Girardeau et al., 2009; Ego-Stengel & Wilson, 2010; Nokia et al., 2010) and leads to the destabilization of task-relevant place fields (Roux et al., 2017). Therefore, it seems plausible that SWRs support the corticohippocampal interactions that drive memory consolidation.

If indeed previous experiences are replayed in the hippocampus and interact with neocortical networks, then replay should also be observed in the cortex. Neurons in various cortical areas, such as entorhinal, mPFC, visual and parietal cortices, show increased firing during SWRs in the sleep periods following an experience (Chrobak & Buzsáki, 1994; Mölle et al., 2006; Ji & Wilson, 2007; Peyrache et al., 2009; Remondes & Wilson, 2015; Khodagholy et al., 2017). These activations reflect experience-related activity from the prior active state (Qin et al., 1997; Ji & Wilson, 2007; Peyrache et al., 2009; Jadhav et al.,

2016; Malvache et al., 2016). Critical to the hypothesis that these reactivations are coordinated between the hippocampus and cortex, they co-occur in time (Ji & Wilson, 2007) and have a similar content (Olafsdóttir et al., 2016). Importantly, hippocampal activity can predict subsequent neocortical patterns and vice versa, which is consistent with a bidirectional communication (Rothschild et al., 2017)

If post-training corticohippocampal interactions during NREM sleep are crucial to the consolidation process, then interfering with them should affect subsequent retention of an experience. Indeed, functional disconnection of the hippocampus and mPFC significantly impairs delayed but not immediate retention of spatial tasks (Floresco et al., 1997; Wang & Cai, 2006). The time course of hippocampal and neocortical activation also agrees with the two-stage consolidation model. Mapping of immediate early gene activation, which reflects neuronal activity, shows an early post-training increase in hippocampal activity and a late increase in neocortical activity (Bontempi et al., 1999). Also, hippocampal inactivation disrupts recent but not remote memories, whereas inactivation of the mPFC or anterior cingulate has the opposite effect, agreeing with an early involvement of the hippocampus and a late role of the neocortex in memory storage (Maviel et al., 2004).

In summary, there are strong corticohippocampal interactions after an experience that reflect its contents and are necessary for successful memory consolidation. These interactions between the hippocampus and neocortex are likely important contributors to the consolidation process.

1.2 Memories are strengthened by emotional arousal

Another significant contributor to memory consolidation is the emotional content of an experience. People that undergo stressful experiences can describe these events in detail long after they occurred (Christianson, 1992). Since emotionally arousing events are usually of key importance, the facilitation of memory by emotions would be highly adaptive, allowing "organisms [to] select from recent experiences those that should be permanently stored" (Gold & McGaugh, 1975, p. 375).

There are several candidate mechanisms for this effect, such as the release of stress hormones during emotional events (Cahill, 2000). Indeed, stress hormone administration after an experience can enhance subsequent memory (Cahill & McGaugh, 1998). As reviewed below, much evidence indicates that the basolateral amygdala (BLA) mediates the enhancement of memory by stress hormones and emotional arousal.

The role of the basolateral amygdala in memory consolidation

While the BLA has often been associated with fear memory formation and storage (LeDoux, 2000; Gründemann & Lüthi, 2015), it has also been implicated in the emotional modulation of memory consolidation in other areas (McGaugh, 2004). In order to investigate this possibility, many studies conducted pharmacological manipulations of the BLA after training in an emotional task. Post-training manipulations are particularly useful when studying consolidation because they cannot affect performance during acquisition.

Supporting the idea that the amygdala is involved in the consolidation process, early studies showed that electrical stimulation of the BLA immediately after aversive training can either boost or impair subsequent memory, depending on the experimental setting (Goddard, 1964; Gold et al., 1975). Furthermore, lesions or inactivations of the BLA conducted up to two days after inhibitory avoidance (IA) training, where an animal learns to avoid a location that was paired with a shock, significantly reduce subsequent retention, while they had no effect at later timepoints (Liang et al., 1982; Zanatta et al., 1997; Huff et al., 2013). Local infusions of tetrodotoxin only have a deleterious effect on retention if done within 90 minutes of IA training (Bucherelli et al., 1992). Post-training BLA manipulations can also enhance memories, with noradrenergic agonist infusions in the BLA enhancing IA retention only when performed shortly after training (Gallagher et al., 1977; Gallagher & Kapp, 1981). These manipulations appear to be specific to the processes supporting long-term memory formation, because post-training BLA inactivation spares short-term retention (McGaugh, 2004; Gale et al., 2004). Similar results have been observed in human epilepsy patients, where amygdala stimulation shortly after the presentation of novel objects can boost memory on next-day, but not same-day retention (Inman et al., 2018). Finally, post-training pharmacological manipulations of the BLA not only affect the consolidation of aversive memories, but also spatial memories potentiated by positive reinforcement (Packard et al., 1994; Packard & Teather, 1998). Overall, there seems to be a restricted time window after training, during which BLA manipulations affect memory retention.

To summarize, BLA plays a pivotal role in the enhancement of long-term memory consolidation. This modulation affects both appetitive and aversive memories. It is also

time-limited, with manipulations that disrupt or enhance memories having the strongest effects shortly after the initial experience.

1.3 Emotional modulation of systems consolidation: anatomical and physiological interactions

Even though the two aforementioned phenomena have largely been studied independently, their anatomical and physiological overlap suggests that they interact, pointing to an integrated mechanism for the emotional enhancement of memory consolidation. This suggests that the brain areas implicated in systems consolidation and emotional enhancement of memory should interact, and those interactions should be associated with activities in the hippocampus.

BLA and mPFC

The BLA and mPFC are reciprocally connected (McDonald, 1998; Rosenkranz & Grace, 2001). mPFC activity mostly excites BLA cells (Likhtik et al., 2005), while BLA inputs can excite mPFC cells but also lead to their feedforward inhibition (Floresco & Tse, 2007; McGarry & Carter, 2016). Communication between the BLA and mPFC is linked to expression of emotional memory. Inhibition of BLA inputs to the mPFC reduces conditioned responses to cues as well as anxiety-related behaviors (Sotres-Bayon et al., 2012; Felix-Ortiz et al., 2016; Klavir et al., 2017), whereas excitation of the same pathway

causes the opposite (Burgos-Robles et al., 2017; Felix-Ortiz et al., 2016). Interestingly, local interneuron inactivation in the BLA can also affect mPFC networks and their responses to fear conditioning (Davis et al., 2017). BLA and mPFC show coordinated activity in the theta band during fear discrimination (Likhtik et al., 2014) and odor fear conditioning (Taub et al., 2018). Gamma activity in the two areas is coupled to theta oscillations (Stujenske et al., 2014). Finally, the glucocorticoid-mediated facilitation of memory consolidation depends upon interactions between the BLA and mPFC (Roozendaal et al., 2009; Barsegyan et al., 2019). Overall, these findings suggest that the BLA is likely in a pivotal position to affect consolidation through modulation of prefrontal activity.

BLA and ventral hippocampus (vHipp)

Based on functional dissociations and anatomy, the ventral hippocampus (vHipp) has been linked to emotional behavior, in contrast to the dorsal hippocampus (dHipp), which is thought to support spatial processing (for a review see Fanselow & Dong, 2010). Indeed, the BLA only has reciprocal connections with the vHipp (Pitkänen et al., 2000). This makes vHipp more relevant to the emotional modulation of memory consolidation.

BLA-hippocampal interactions play an important role in consolidation. For example, BLA lesions abolish the memory enhancing effect of glucocorticoid infusions in the hippocampus (Roozendaal & McGaugh, 1997). Furthermore, hippocampal inactivation blocks the memory boosting effects of the BLA after training in a spatial task (Packard & Teather, 1998). Importantly, 40-Hz stimulation of BLA projections to the vHipp after

contextual fear conditioning enhances footshock retention, while inactivation of the same projections has the opposite effect (Huff et al., 2016).

Besides an explicit role in emotional memory consolidation, the interaction between these structures is also affected during emotional memory retrieval and anxiety behaviors. In terms of task-related activity, BLA and ventral CA1 show coordination in the theta band during presentation of an auditory stimulus associated with a shock (Seidenbecher et al., 2003). This coordination only appears during long-term, but not short-term memory retrieval (Narayanan et al., 2007), which indicates that the BLA can influence the retrieval of long-term memories. Similar results were obtained in epilepsy patients, with enhanced theta coupling between amygdala and hippocampus during the presentation of aversive stimuli (Zheng et al., 2017). Finally, BLA neurons projecting to the vHipp show elevated activity during fear renewal (Orsini et al., 2011), and the same projections mediate both anxiety-related and social behaviors (Felix-Ortiz et al., 2013; Felix-Ortiz & Tye, 2014).

vHipp and mPFC

The important interactions between the hippocampus and the mPFC in memory consolidation have already been covered (see Section 1.1). What should be mentioned though is that most hippocampal projections to the mPFC originate in the vHipp. In fact, vHipp-mPFC interactions are involved in anxiety and fear discrimination behaviors (Adhikari et al., 2010; 2011). Furthermore, inhibiting vHipp projections to the mPFC can reduce anxiety behaviors (Padilla-Coreano et al., 2016) and suppress fear renewal (Marek et al., 2018). Indeed, neurons in vHipp that are activated during an anxiogenic situation

tend to project to mPFC (Ciocchi et al., 2015). Thus, these monosynaptic connections close the loop of direct interactions between all the areas involved in emotional modulation of memory consolidation.

1.4 Hippocampal population events: roles in memory consolidation

Neurons throughout the hippocampal formation exhibit coordinated population bursts that may play a role in the memory consolidation process. During quiet rest and slow wave sleep (i.e. NREM), the behavioral states most associated with declarative memory consolidation, the hippocampus exhibits two particularly promising phenomena, dentate spikes (DSs), seen in the dentate gyrus, and SWRs in the CA1. We already covered the literature on the importance of SWRs in memory consolidation. Now, I will explain the mechanisms of SWR and DS generation, as well as their interaction with the neocortex, the putative permanent storage site of declarative memories.

Sharp wave ripples (SWRs)

SWRs are composed of two concomitant events: a sharp wave, which is a brief (~50 ms) negative potential in stratum radiatum of hippocampal field CA1 (Buzsáki, 1986), and a superimposed ripple, which is a brief burst of fast (140-200 Hz) oscillations generated in the CA1 pyramidal layer (Buzsáki et al., 1992). Sharp waves result from the synchronous bursting of CA3 pyramidal cells, which drive a post-synaptic depolarization of the apical

dendrites of CA1 pyramidal cells (Buzsáki et al., 1992; Csicsvari et al., 2000). This synchronous excitatory input results in the fast oscillatory recruitment of CA1 principal cells and inhibitory interneurons, generating the ‘ripple’ (Buzsáki et al., 1992; Ylinen et al., 1995).

As described previously, neocortical activity in various areas is increased around SWRs (Sirota et al., 2003; Mölle et al., 2006; Remondes & Wilson, 2015; Headley et al., 2016; Malvache et al., 2016; Rothschild et al., 2017). This is clearly visible in the case of the mPFC, which shows robust activity during these events (Peyrache et al., 2011; Headley et al., 2016; Jadhav et al., 2016). These mPFC-hippocampal interactions are particularly important for memory consolidation (Maingret et al., 2016).

Only one study examined the interaction between SWRs and BLA activity. It showed that a percentage of BLA cells were significantly modulated during SWRs. These modulated BLA cells along with hippocampal cells formed ensembles that reflected prior learning upon reactivation (Girardeau et al., 2017). This result is not surprising, given the monosynaptic connections between CA1 and BLA. Indeed, the ventral CA1 cells that are preferentially activated in relation to SWRs send collaterals to the BLA (Ciocchi et al., 2015). In addition, stimulation of the hippocampus affects plasticity in the BLA (Maren & Fanselow, 1995). This indicates that hippocampal SWR-related activity may induce plasticity within the BLA (Sadowski et al., 2016).

Dentate spikes (DSs)

Dentate spikes are generated in the dentate gyrus, and their role in memory formation has not been investigated. In extracellular recordings, they appear as large positive voltage events lasting 5 to 10 ms and are mostly seen during offline states (Bragin et al., 1995a; Headley et al., 2016). During such states, the principal input to the dentate gyrus, the entorhinal cortex, emits bursts of activity (Paré et al., 1995). DSs are likely driven by these bursts because they are eliminated by entorhinal lesions (Bragin et al., 1995a). Also consistent with initiation by the entorhinal cortex, DSs are associated with activation of the granule cell layer of the dentate (Colgin et al., 2004), and *in vivo* intracellular recordings have shown that they coincide with synaptic depolarizations of granule cells and hilar interneurons (Penttonen et al., 1997). This particular pattern of activation is consistent with the extracellular voltage profile of DSs (Fernández-Ruiz et al., 2013). Furthermore, unit activity, gamma band power, and coherence throughout the cortex are elevated around DSs (Headley et al., 2016), suggesting that they depend upon widespread coordinated cortical activity extending beyond the entorhinal region. It was proposed that DSs gate hippocampal output by activating inhibitory neurons in the hilus that project to CA1 (Penttonen et al., 1997). Indeed, the rate of CA1 SWRs is transiently diminished shortly after DS occurrence, although the coincident activation of entorhinal inputs to CA1 could contribute to this effect as well (Bragin et al., 1995a; Penttonen et al., 1997; Headley et al., 2016). In general, DSs are important for memory processing, since disrupting communication between the dentate gyrus and CA1 when DSs occur affects memory both positively and negatively in various tasks (Nokia et al., 2017; Lensu et al., 2019). Furthermore, dentate lesions reduce SWR occurrence after appetitive learning (Sasaki et

al., 2018). As a result, DSs are in a position to modulate SWRs. Thus, DSs could participate in memory consolidation, although it is presently unclear if they do so in the same manner as SWRs.

1.5 Gamma oscillations: mediators of interregional interactions

In order for a novel experience to be successfully consolidated, the newly acquired information needs to be transferred between brain regions. Neuronal oscillations are thought to provide the temporal coordination that is necessary for this transfer (Buzsáki &

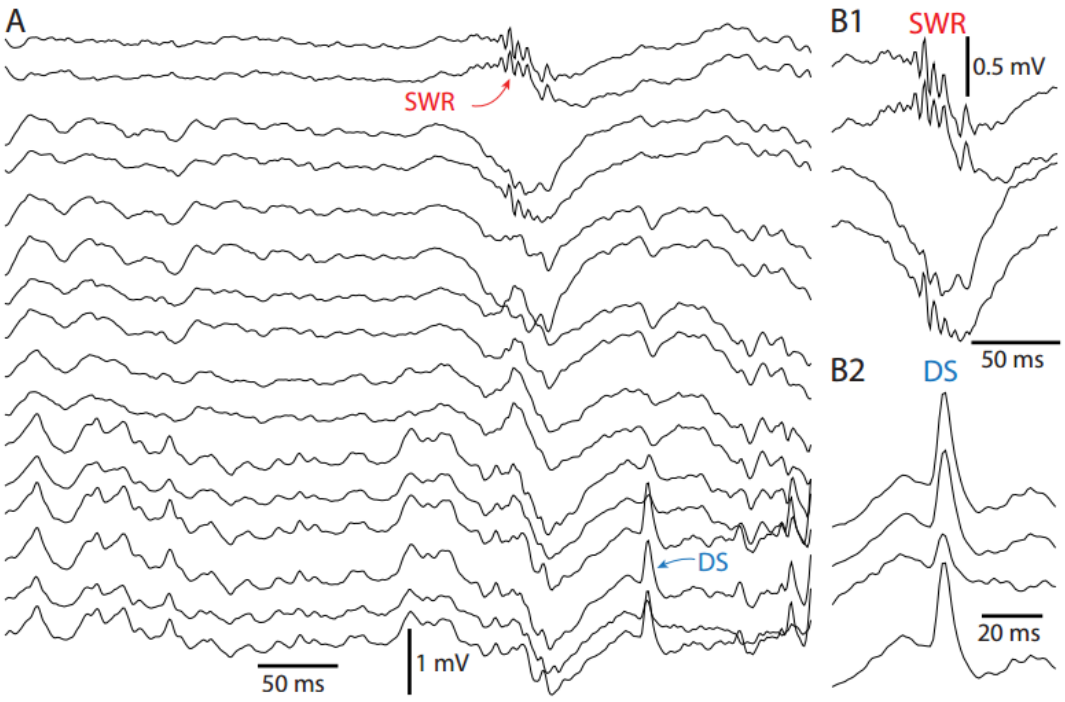

Figure 1-1: Example traces of SWRs (A, red, B1) and DSs (A, blue, B2). Figure from Headley, Kanta & Paré, 2016.

Schomburg, 2015). Many brain areas, such as the neocortex, striatum, and olfactory bulb, display field potential oscillations between 30 and 100 Hz (termed gamma) that entrain local unit activity (Buzsáki & Wang, 2012).

Presence of gamma oscillations in areas involved in consolidation

Gamma oscillations are present in all regions involved in the emotional modulation of memory consolidation. In the BLA, bursts of gamma occur spontaneously under anesthesia (Collins et al., 2001) and during emotional tasks (Likhtik et al., 2014; Popescu et al., 2009; Courtin et al., 2014; Amir et al., 2018; for review see Headley and Paré, 2013). These bursts coordinate the spiking of neurons in the BLA and regions it is connected with, like the perirhinal cortex (Collins et al., 2001) and striatum (Popescu et al., 2009). Gamma-associated coupling also extends to the mPFC and vHipp, which exhibit gamma band coherence with the BLA (Stujenske et al., 2014). In fact, BLA cells projecting to the mPFC are more strongly entrained by gamma than those projecting to nucleus accumbens (Amir et al., 2018). The mPFC and vHipp also show robust gamma oscillations (Siegel et al., 2009; Traub et al., 1996; Penttonen et al., 1998; Trimper et al., 2017), which can be modulated by BLA activity (Bass & Manns, 2015; Inman et al., 2018)

The amplitude of gamma oscillations is often modulated by the phase of lower frequency rhythms, in particular theta. In the hippocampus, this coupling segregates slow and fast gamma into different temporal epochs (Colgin, 2015; Colgin et al., 2009). Interestingly, these gamma bands are generated by distinct hippocampal inputs, implying that theta can sequence the information exchange mediated via gamma (Colgin et al., 2009; Schomburg et al., 2014). A similar theta-gamma coupling has been reported in the BLA,

vHipp, and mPFC (Stujenske et al., 2014). Thus, gamma oscillations are in a position to mediate interactions between these three structures during consolidation.

1.6 Mechanisms of gamma generation

Gamma oscillations are a population-level phenomenon arising from the local interactions between neurons and their extrinsic drive. Numerical simulations have established that the minimum components necessary for gamma generation is an excitatory drive onto a network of reciprocally connected inhibitory interneurons with $GABA_A$ inhibitory post-synaptic potentials (IPSPs, Wang & Buzsáki, 1996). Since that excitation can be extrinsic or from local principal cells, two models are commonly proposed for gamma generation, namely the Interneuron Network Gamma (ING) model and the Pyramidal Interneuron Network Gamma (PING) model.

Interneuron Network Gamma (ING)

This model requires interneurons inhibiting each other via synapses with a fast decay time constant (i.e. $GABA_A$), and sufficient external drive to fire the interneurons despite the recurrent inhibition (Buzsáki & Wang, 2012). ING can be elicited *in vitro* by isolating interneurons from phasic inputs through ionotropic glutamate receptor blockade, and then inducing a tonic depolarization (Whittington et al., 2011), for example through muscarinic receptor activation (Buzsáki & Wang, 2012). In the ING model, the oscillation frequency

is dependent on the strength of the tonic inputs to the interneurons, as well as their resonant properties (Traub et al., 1996). While fluctuations in the amount of drive can result in unstable oscillation frequencies, gap junctions between interneurons might act as a stabilizing mechanism (Traub et al., 2004).

Pyramidal Interneuron Network Gamma (PING)

In PING, gamma arises from reciprocal interactions between excitatory principal cells and inhibitory interneurons (Whittington et al., 2011). PING models are more relevant than ING models for the BLA (Feng et al., 2019), mPFC, and vHipp because each region contains both glutamatergic and GABAergic neurons. In PING models, gamma arises from a continuous alternation between excitation and feedback inhibition. The delays necessary for the emergence of gamma match the ones observed experimentally, including the onset and offset kinetics of $GABA_A$ and AMPA currents.

Central to ING and PING is fast perisomatic inhibition provided by fast-spiking parvalbumin (PV) immunopositive basket cells (Sohal et al., 2009). Indeed, the autocorrelation functions of histologically verified PV cells show resonance at gamma frequencies (Bragin et al., 1995b). Furthermore, optogenetically driving PV cells at gamma frequencies increases gamma power in the local field potential of the barrel cortex (LFP, Cardin et al., 2009).

1.7 Functions of gamma oscillations

What is the function of gamma oscillations? Given that they operate on the time scale of postsynaptic integration, two possibilities stand out: one is that they facilitate the induction of synaptic plasticity by enabling presynaptic neurons to reliably elicit postsynaptic spikes. The other is that they enable the efficacious transmission of signals between brain regions both by summating postsynaptic potentials and synchronizing their periods of depolarization that oscillate coherently.

Synaptic plasticity

An important characteristic of gamma oscillations is that they telescope periods of effective synaptic interactions into short time windows, ideal for the induction of long-term potentiation and spike timing dependent plasticity (Markram et al., 1997; Bi & Poo, 1998). Indeed, studies have shown that the timing of spikes, as well as the perisomatic location of inhibitory inputs on pyramidal cells during gamma match the requirements for the induction of synaptic plasticity (Traub et al., 1998). Furthermore, timing external stimulation to specific phases of the gamma cycle can lead to either synaptic potentiation or depression (Wespatat et al., 2004; Ni et al., 2016). Moreover, gamma oscillations produce cell type-specific plasticity in CA3 cells *in vitro* (Zarnadze et al., 2016). Importantly, the amplitude of gamma oscillations during auditory fear conditioning predicts receptive field-specific plasticity 24 hours later (Headley & Weinberger, 2011). Thus, gamma oscillations are a likely candidate for the spatiotemporal coordination of neuronal activity that supports the formation of memory traces.

Communication through coherence (CTC) hypothesis

As mentioned before, oscillations are considered important coordinators of information transfer. A widely accepted hypothesis, communication through coherence (CTC), stipulates that gamma is the ideal rhythm for gating the exchange of information between brain regions. In this model, two brain areas most effectively communicate with each other when their oscillations are coherent, due to their co-fluctuations in excitability within the gamma cycle (Fries, 2005; 2015). This contrasts with information transmission through firing rate-based codes, which do not drive downstream targets as effectively, because inputs arrive at random phases of neuronal excitability. On the other hand, coherent gamma oscillations corral spikes together so that they reach target neurons when they are most excitable, enhancing their impact.

This mechanism also explains why areas can tune in to particular inputs and effectively ignore others. Essentially, if an area oscillates at a particular frequency, this will make similar incoming rhythms ideal for effective communication, due to the timely arrival of spikes within the gamma cycles. This type of interaction will lead to fast transmission of a large amount of information (Buehlmann & Deco, 2010; Rohenkohl et al., 2018). In contrast, improperly timed inputs will have little to no effect (Fries, 2015; Buzsáki & Schomburg, 2015; Rohenkohl et al., 2018). The CTC hypothesis can also explain why synaptic delays between upstream and target regions do not necessarily affect this communication, because an input from one oscillation cycle can arrive downstream at the high excitability phase of the next cycle. This might mean that fixed conduction delays between different regions result in different resonant gamma frequencies.

Besides compressing spiking into packets optimal for postsynaptic integration, gamma oscillations also provide “rapid balancing” of excitation and inhibition, because they emerge from the dynamic interaction between principal cells and inhibitory interneurons (Fries, 2015). Indeed, cortical and hippocampal networks both exhibit a balance of excitation and inhibition during active states (Shu et al., 2003; Haider et al., 2006). The amount of excitation and inhibition can change, albeit maintaining their ratio. Slight variations in this ratio change the frequency and amplitude of gamma oscillations (Atallah & Scanziani, 2009).

A good example of CTC supported by gamma comes from the hippocampus, where CA3 and CA1 interact at slow gamma frequencies, whereas the entorhinal cortex and CA1 show coherent fast gamma (Colgin et al., 2009). In fact, these two gamma bands provide different representations, with slow gamma being associated with future trajectories in space, and fast gamma linked to current location in time (Zheng et al., 2016). In this case, coherence is selectively increased between different pairs of regions depending on which area is recruited more intensely. However, an important caveat to interpreting changes in coherence between two areas is that they are not always an indication of interregional interactions, because they can also reflect the influence of a third area entraining both targets (Buzsáki & Schomburg, 2015).

1.8 Memory correlates of gamma oscillations

The hippocampus and neocortex display strong gamma oscillations during mnemonic processing. Gamma oscillations participate in object representation, showing a sustained presence during the delay period in a delay matching-to-sample task (Tallon-Baudry et al., 1999) and increasing during post-learning slow wave sleep (Mölle et al., 2004). Furthermore, the levels of gamma synchronization between rhinal cortices and hippocampus during word encoding in humans predict if a word will be successfully recalled (Fell et al., 2001). Similarly, gamma amplitude in the hippocampus and frontal cortex during encoding correlates with subsequent memory strength (Sederberg et al., 2007). Interestingly, cells encoding a successfully recalled object show stronger phase locking to gamma (Jutras et al., 2009). Finally, gamma power and coherence between CA3 and CA1 is increased around SWRs, with higher levels of coherence correlating with more reliable replay of recently encoded experiences (Carr et al., 2012). Overall, gamma oscillations likely play an important role in the encoding of important information. Similar mechanisms are likely to arise during consolidation, resulting in the efficient transmission of information to long-term storage.

Consistent with a role in the emotional enhancement of memory, gamma oscillations appear frequently during emotional experiences, such as the presentation of fearful stimuli (Headley & Paré, 2013). In humans, gamma power in the amygdala and many cortical areas is increased in the presence of noxious conditioned or unconditioned stimuli (Miltner et al., 1999; Sato et al., 2011). Besides being simply present during a

fearful experience, gamma in the BLA correlates with subsequent memory strength. For example, coherence between BLA and rhinal cortex (Bauer et al., 2007) or BLA and striatum (Popescu et al., 2009) during conditioned stimulus (CS) presentations predicted subsequent retention. Furthermore, gamma oscillations in the auditory cortex during CS presentation early in training correlate with the strength of the CS-US association that forms (Headley & Weinberger, 2011). Crucial to the potential role of gamma oscillations in consolidation, optogenetic stimulation of the BLA at gamma frequencies results in enhanced consolidation of contextual memory, whereas tonic optogenetic inhibition, which ostensibly blocks gamma, has a deleterious effect (Huff et al., 2013; 2016). Similarly, electrical stimulation of the BLA in epilepsy patients after novel object presentation increases gamma coordination between hippocampus and cortex as well as long-term memory retention (Inman et al., 2018).

Overall, the evidence reviewed above suggests that gamma oscillations in the BLA participate in the consolidation of emotional memories, possibly by facilitating communication between the BLA and other areas directly related to the consolidation process. More specifically, after an emotionally arousing experience, gamma oscillations in the BLA likely excite downstream consolidation-related targets such as vHipp and mPFC. This synchronized activity of the two areas allows for the effective transmission of experience-related information, through systems consolidation. A possible marker of this interaction would be increased gamma coherence between some of the aforementioned pairs of areas.

CHAPTER 2

General Materials and Methods

2.1 Surgery

Adult male Long Evans rats (300-500 g, Charles River Laboratories, Fairfield, NJ) were anesthetized with ~2% isoflurane (Henry Schein, Melville, NY) and placed in a stereotaxic frame (Kopf Instruments, Tujunga, CA). After the skull was exposed and cleaned, craniotomies were performed over the sites where the electrodes would be placed (BLA: AP -2.52, ML +5, DV -7.5 from brain surface; mPFC: AP +3.24, ML +0.6, DV -4; CA1: AP -6, ML +6, DV –6; Dentate Gyrus (DG): AP -6, ML +4 DV -4.8). Tungsten wire tetrode arrays or single wires (20 or 50 μm diameter, California Fine Wire, Grover Beach, CA) were either inserted and fixed in place or advanced towards their target using chronically implanted 3D-printed microdrives (Headley et al., 2015). For optogenetic experiments, an

optrode was inserted instead of an electrode array. The optrode consisted of a single tungsten wire or tetrode attached to a 200 μm, 0.39 NA optic fiber, coupled with a 2.5 mm FC/PC ceramic ferrule (Thor Labs, Newton, NJ). The vertical distance between the fiber and electrode tips was ~1.5 mm. Electromyographic (EMG) and electroencephalographic (EEG) activities were also recorded using stainless steel skull screws. For silicon probe recordings, a probe with an 8x8 array of recording sites (200 μm spacing) was inserted into the BLA and oriented in the coronal plane. Electrodes, optrodes, skull screws and electrode interface boards (EIBs, Neuralynx Inc., Bozeman, MT) were secured to the skull using dental cement (Teets Denture Material, Co-Oral-Ite, Diamond Springs, CA). All procedures were approved by the Institutional Animal Care and Use Committee (IACUC) of Rutgers University, in compliance with the Guide for the Care and Use of Laboratory Animals (Department of Health and Human Services).

2.2 Recording of spontaneous activity

Once subjects fully recovered from the surgery, spontaneous activity across sleep/wake cycles was recorded, for at least four hours per day for two days. All recordings were conducted in a box to which the animals were fully acclimated (“home box”). This was a square (2 ft x 2 ft x 2 ft), black, enclosure with paper towel bedding on the floor, and dim illumination (2 lux).

2.3 Inhibitory Avoidance (IA) paradigm

Spontaneous BLA activity was recorded for one hour (Pre-Training) in the "home box". Then, rats underwent IA training. The subjects were placed in a rectangular alley (**Fig. 4-1A**) comprised of a brightly lit (1500 lux) compartment (52 cm (L)-25 cm (W)-30 cm (H)) connected to a dark (200 lux) section with a shock grid floor (29 cm (L)-35 cm (W)-30 cm (H)). The subjects' latency to enter the dark compartment was measured. To be scored as an entry, all paws had to touch the shock grid. After entering the dark compartment, re-entry into the light compartment was blocked by a sliding door and an electric footshock was delivered (1 mA for 1 sec, Coulbourn Instruments, Holliston, MA). Immediately following training, BLA activity was recorded for another hour in the "home box" (Post-Training). Retention was tested 48 hours later by placing the subjects in the light compartment and measuring the latency to enter the dark section, with a cutoff point of 300 seconds. During this recall test, no shock was administered. Performance was measured as the difference between retention and training latencies. Subjects were divided into Good Learners and Poor Learners based on a median split of their performance distribution.

2.4 Hole-board foraging task (HB) paradigm and recordings

The HB task was adapted from a previously described version (Bast et al., 2005) with some modifications. The arena was a 180x180 cm square table with 6x6 equidistant sand wells

(10 cm diameter, 12 cm depth) forming a square grid (**Fig. 5-1A,B**). On all sides of the apparatus, there were salient visual cues and starting boxes (20x10 cm) with a sliding door leading to the maze (**Fig. 5-1A**). The four sides were named North, East, South and West. Animals were placed on food restriction (14g of rat chow per day, maintaining at least ~85% of initial body weight) for the entire duration of the experiments. After a few days of restricted access to food, rats were habituated to retrieving buried food pellets from sand wells inside their home cages (Pre-Training stage 1). After 3 days of exposure, animals that did not retrieve the pellet within 5 minutes were excluded. The remaining animals were exposed to the HB arena and trained to forage (Pre-Training stage 2). During this stage, only one out of 36 wells was accessible, while the rest had a lid on top of them. A visible food pellet was placed on the surface of the open well. Animals received four trials each day. In every trial, rats were placed in a start box and the door slid open, giving them access to the arena for five minutes. Both the start box and baited food well differed on every trial. Latency to retrieve the pellet was noted.

Once rats acquired the concept of foraging in the maze, as evidenced by decreased latencies to retrieve the food pellet, they continued into Pre-Training stage 3, where the uncovered baited well remained the same for the four trials, except that on the last trial the pellet was buried. Rats were trained on this version until they showed short latencies (< 2 mins) to the correct well and retrieved the buried pellet on the last trial. Rats that did not show adequate performance were excluded from the next phase.

Once rats were fully acclimated to the procedure, they were introduced to the final experimental phase of the task (**Fig. 5-1B**). In this phase, 5 out of 36 holes were uncovered on every training day, with only one of them containing the food reward. Rats underwent

four trials every day. On trial 1 (Training Trial), the pellet was visible on the surface of the sand well. On trials 2-4 (Retention Trials), the pellet was either buried or absent (Probe Trial). Probe Trials were restricted to the third or fourth trial, so that rats could not predict when they would take place. Various precautions were taken to make sure that rats did not rely on any proximal cues, such as odor, to solve the problem: (1) mixing finely ground food into all sand wells, (2) using different start boxes on every trial, and (3) rotating the arena between trials while keeping the position of the baited well constant with respect to the distal cues. Furthermore, the outside rows of sand wells were not used, because their proximity to the walls could encourage thigmotaxis. Various Training-Retention intervals were tested (**Fig. 5-1D**), but the interval used for all modulation trials was 1 hour. Latency to approach the correct well was measured on all trials and was normalized with respect to the first trial performance (Latency on trial N/Latency on trial 1).

2.5 Virus injections

Optogenetic control of neural activity was achieved with an adeno-associated viral vector (AAV) driving the expression of the Chronos channelrhodopsin variant (Klapoetke et al., 2014), under a Synapsin promoter (AAV5.hSyn.Chronos-GFP, UNC Vector Core, Chapel Hill, NC). Virus infusions (200 nl) were performed in the BLA using a pressure injector (Nanoject III, Drummond Scientific Company, Broomall, PA) and glass micropipettes (Narishige, Amityville, NY). After waiting for ~2 months to allow for full expression,

implant surgeries were performed (see 2.1). During this time, animals were pre-trained in the HB task. On a subset of animals, *in vitro* experiments were performed (see 2.6).

2.6 Whole-cell recordings of BLA neuron in brain slices kept *in vitro*

To characterize the impact of Chronos activation, whole-cell patch recordings were obtained from BLA neurons. Rats were sacrificed with an overdose of isoflurane. Their chest cavity was opened, and they were perfused through the heart with a modified cold artificial cerebrospinal fluid (aCSF) for 30 seconds. The modified aCSF was comprised of (mM): 103 N-methyl-D-glucosamine, 2.5 KCl, 1.2 NaH_2PO_4, 30 $NaHCO_3$, 10 $MgSO_4$, 25 glucose, 20 HEPES, 101 HCl, 2 Thiourea, 3 Na-Pyruvate, 12 N-acetyl-L-cysteine, and 0.5 $CaCl_2$. Rats were then decapitated and their brain was quickly removed, blocked, and sliced with a vibrating microtome (Dosaka, Kyoto, Japan) at a thickness of 300-400 μm starting at the anterior pole of the BLA. The cutting solution was the same cold modified aCSF mentioned above. Slices were then transferred to a chamber containing modified aCSF at 32° C for five minutes, after which they were moved to a holding chamber at room temperature (22° C) with normal aCSF (mM, 124 NaCl, 2.5 KCl, 1.25 NaH_2PO_4, 26 $NaHCO_3$, 1 $MgCl_2$, 2 $CaCl_2$, and 10 glucose, pH 7.2-7.3, 305 mOsm). Slices were kept in the holding chamber for at least an hour prior to recording.

To obtain whole-cell patch recordings, a slice was transferred to the recording chamber where aCSF heated to 32° C continuously flowed. Slices were immobilized under a nylon net. A patch pipette (resistance 5-8 MΩ) filled with intracellular solution (mM: 130 K-

gluconate, 10 N-2-hydroxyethylpiperazine-N'-2'-ethanesulfonic acid, 10 KCl, 2 $MgCl_2$, 2 ATP-Mg, and 0.2 GTP-tris(hydroxy-methyl)aminomethane, pH 7.2, 280 mOsm) was guided towards a neuron with infrared video microscopy at 60X (Axioskop, Zeiss, Thornwood, NY). We did not correct for the liquid junction potential, which for this solution is 10 mV. Neuronal activity was recorded in current-clamp mode using a Multiclamp 700B amplifier and digitized the signal with a Digidata 1550 (Molecular Devices, San Jose, CA).

Once the membrane potential stabilized, a graded series of 500 ms current pulses was delivered, ranging from -200 to 360 pA in 40 pA steps. The first action potential evoked by the largest current pulse was used to classify neurons as either principal cells (PN) or fast-spiking interneurons (FS). Neurons with action potential halfwidths <0.35 ms were classified as FS.

To assess optogenetic responsiveness, blue light stimuli were delivered for either 2, 5, or 500 ms. These could occur as either single pulses (2 or 500 ms) or trains of stimuli (5 ms pulses at 8 or 20 Hz for 1 s; 2 ms pulses at 50 Hz for 1 s). When classifying the optogenetic responsiveness of neurons, if a cell consistently emitted an action potential in response to any optogenetic stimulus, it was classified as spiking. If the neuron exhibited a rapid and sustained depolarization from rest, but no spiking, in response to the 500 ms current pulse, it was classified as having just a photocurrent. Last, some neurons exhibited a hyperpolarization upon delivery of blue light. In a subset of these cells, we tested whether their response was mediated by GABAergic synapses by adding picrotoxin (100 μM) to the perfusate.

2.7 Processing stages for closed-loop controller

The closed-loop control algorithm was programmed in LabView and implemented on a USB-7845 reconfigurable multifunction data acquisition module (National Instruments, Austin, TX). A Kintex-7 70T field programmable gate array (FPGA) on the device instantiated the algorithm. Because the FPGA generates dedicated circuits for each processing step, the algorithm can run as fast as the clock rate of the chip, which is 80 MHz.

1. Analog to digital conversion: Signal is acquired as a fixed-point number (27 bits for digits, 5 bits for the scaling factor) and converted to a 32-bit signed integer to lower the logic overhead associated with numerical operations.

2. Clocking the algorithm: Processing goes in 40 μs steps, yielding an updating frequency of 25 kHz.

3. Obtaining the amplitude and phase: This module implements a bank of filters followed by control circuitry. The signal is passed separately to each filter with center frequencies at 35, 55, 75, and 95 Hz. For the purpose of the described experiments, the only filter used was the one with 55 Hz as its center frequency. Within a band, two different bandpass filters are used:

a. To detect the phase, the signal is bandpass-filtered with a Butterworth filter (order 2, cutoff frequency g±15 Hz). If the filtered signal crosses from positive to negative, it is denoted as the descending phase, or if the filtered signal goes from negative to positive, it

is denoted as the ascending phase. To detect peaks and troughs, the derivative of the filtered signal was used (with a lag of 2 ms between samples to reduce spurious detections). If this signal crosses from positive to negative a peak is registered, while if it crosses from negative to positive a trough is noted.

b. To detect amplitude, the signal is bandpass-filtered with a Butterworth filter (order 4, cutoff frequency g±15 Hz) and the absolute value of the filtered signal is taken. When either a trough or a peak is detected, then the amplitude value is updated.

A lower-order filter was used for phase detection to decrease phase distortion. A higher-order filter was used for amplitude detection to increase the frequency specificity of the estimated power in a particular band.

4. Restricting delivery to gamma bursts: To restrict the delivery of light-triggering pulses to gamma bursts, an amplitude threshold was set, as well as a minimum number of cycles that needed to exceed that threshold. This was true for all conditions where gamma levels were tracked (Trough, Peak, Sham, also see Light Delivery section). Each day the amplitude threshold was set during the Light OFF condition so that on average pulses were delivered at 20 Hz (**Fig. 7-3A,B**). In order for the triggering to start during a gamma burst, at least 2 cycles had to occur above threshold. A maximum number of pulses to deliver per burst could also be set (for instance, to restrict delivery to 1 pulse per gamma burst), but this value was set to 1000, which is effectively no maximum.

5. Light delivery: Triggering pulses were passed to a module that generated a 2 ms long digital output to drive a blue LED. A minimum interval of 10 ms was imposed between pulses, to avoid delivering more than one pulse per gamma cycle or retriggering

on the light-evoked LFP response. Four different light delivery protocols were used: pulses were either delivered at the trough (Trough treatment), peak (Peak treatment), randomly with an average frequency of 20 Hz (Random treatment) or during gamma but with light delivery blocked at the fiber stub (Sham treatment). The light source for the optogenetic experiments was a PlexBright compact LED module with blue light (465 nm - 24.9mW - 792mW/mm2, Plexon Inc., Dallas, TX). The LED module was coupled to a ferrule on the animal's head through a PlexBright Dual LED 16 Channel Commutator and an FC/PC patch cable (Plexon Inc., Dallas, TX). Light intensity was adjusted in each animal so that 2 ms pulses evoked a positive field potential of ~30 μV. The light intensity at the fiber stub required to elicit this field response was ~2.6 mW.

2.8 Validation of closed-loop accuracy

A function generator (AFG1062, Tektronix, Beaverton, OR) was used to produce a sinusoidal waveform with a continuously ascending frequency from 1 – 200 Hz, known as a chirp. The amplitude of the signal was attenuated to the range of the preamplifiers and it was used to drive the closed-loop algorithm. By simultaneously recording the output of the function generator and the triggering of the algorithm, any lags or distortions introduced by the preamplifier, analog-to-digital converter, and the signal processor could be directly accessed.

2.9 Histology

At the end of the experiments, electrolytic marking lesions (10 μA, 10 sec, A-M Systems, Sequim, WA) were performed for subsequent histological verification of electrode placement. Under deep isoflurane anesthesia, rats were perfused through the heart and their brain was removed and placed in fixative (4% paraformaldehyde in PBS, Sigma Aldrich, St Louis, MO). Two days later, the brain was transferred to a 30% sucrose solution (Sigma Aldrich, St Louis, MO). A few days later, the brain was sectioned on a freezing microtome (80 μm slice thickness, Reichert, Depew, NY). Sections were mounted on gelatin-coated slides and stained with thionin for determination of optic fiber and electrode placement. Some sections were left unstained and coverslipped to verify viral transfection on a confocal microscope (Fluoview FV1000, Olympus, Waltham, MA).

2.10 Recording and data processing

Unit activity and LFPs were recorded with either a Plexon or an Intan recording system (30 kHz/channel sampling rate, Plexon Inc., Dallas, TX/Intan Technologies, Los Angeles, CA) through 16-channel or 96-channel EIBs (Neuralynx, Bozeman, MT) on the animal's head. The resulting binary files were then processed offline using NDManager (Hazan et al., 2006) and MATLAB (Mathworks, Natick, MA).

Unit activity was detected and sorted based on the spike waveforms using KlustaKwik (Harris et al., 2000) and then manually clustered using Klusters (Hazan et al., 2006). For clustering, only the first four principal components were used for each electrode. A waveform cluster was considered a unit if it had a refractory period in its auto-correlogram, as well as a characteristic waveform shape (negative followed by positive deflection) that did not resemble typical artifact/EMG shapes. Single units were isolated based on a refractory period of several milliseconds and a low percentage of overlap with other units at the site (<10%). Pooling all detected units together yielded multiunit activity (MUA). All analyses were restricted to sessions that had a stable MUA/single unit presence throughout the session (>99%).

For peri-stimulus time histograms (PSTH) of unit activity, the baseline for z-scoring included a window of 2 seconds before and after the PSTH. A histogram was considered significant if two consecutive bins deviated by more than 5 SD from baseline in either direction.

For LFP analyses, a Butterworth lowpass filter with a 300 Hz cutoff point (2^{nd} order filter) was used in both forwards and backwards directions to avoid phase distortion. The LFP was then down sampled to a 1kHz sampling rate. Recordings that had high EMG or electrical noise were excluded from spectral analyses.

For phase locking analyses, the pairwise phase consistency (PPC) (Vinck et al., 2010) of the MUA to mid-gamma was calculated. The LFP was filtered between 40 and 70 Hz only in the forward direction, to avoid contamination by the light-evoked LFP response. Phase information was extracted from the filtered trace and MUA phase locking was calculated.

Change in PPC was calculated as the difference between Light ON and Light OFF PPC for any gamma cycle. Spiking probability per phase was calculated as the average firing rate per gamma cycle at any phase. Then, the mean spiking probability was subtracted from all phases to show deviation from the mean.

Frequency spectra were calculated using Welch's power spectral density estimate. A power law function was fitted to the raw spectrum and then subtracted from it to show residual power, accounting for overall changes in spectral power and individual differences. Maximum changes in spectral power and corresponding frequencies were calculated by finding the local maximum in the difference spectra (Light ON minus OFF) between 40 and 70 Hz.

Time-frequency spectrograms and coherograms for Figs 3-1, 3-2, 4-1, 4-2 and 5-2 were calculated using the Chronux package (Bokil et al., 2010) for MATLAB. Spectral power on the LFP time series was computed using a multi-taper technique, for multiple estimates of power within a fixed frequency band and time window. In all spectral analyses, 5 tapers were used. For Figs 3-1 and 3-2 the window size was 0.2 s, overlapping by 25 ms. For Figs 4-1, 4-2 and 5-2, the window size was 2 s, overlapping by 250 ms. For baseline IA and HB analyses, baseline was 30 minutes prior to training. For optogenetic experiments, baseline was the entire Light OFF period.

Time-frequency spectrograms as well as average spectral amplitudes for Figs 6-2 and 6-3 were calculated using Morlet wavelets ranging from 1 to 256 Hz in quarter octave steps. The width of the wavelet was seven cycles. To measure the amplitude at a particular

frequency and time, the absolute value of the complex valued frequency domain representation of the signal was used.

For individual burst analyses, the LFP was filtered in the forward direction to avoid backward contamination by the light-evoked response, and burst cycle numbers and amplitudes were extracted during periods when light pulses were delivered. For each light-modulated burst, 3 cycles before and after the light delivery were also extracted to show specificity of light effects. Changes in amplitude and incidence were calculated based on differences from the Light OFF period.

For analyzing the synchrony of gamma bursts along the dorsoventral axis, data obtained from the subjects implanted with an 8x8 silicon probe in the BLA was used. Mid-gamma bursts were detected in the wavelet power spectrogram at a site midway along the shank. The time of each burst corresponded to the trough of the oscillation that was nearest to a local peak in the power of the spectrogram. By taking the mean LFP waveform (window ±75 ms) of across all sites at these peak times mid-way along the shank we could visualize the synchrony in gamma across recording sites. The distribution of phases in the wavelet spectrogram was obtained at each site by applying the angle function to the complex valued wavelet spectrogram at the peak times.

Recordings from the 8x8 silicon probes were also subjected to current source density (CSD) analysis to determine whether the sources underlying the LFP gamma observed in the BLA were local. Due to the non-laminar structure of the BLA, and the two-dimensional arrangement of recording sites, the inverse current source density technique was used to obtain estimates of the CSD (Leski et al., 2011). Unlike traditional approaches that take

the second spatial derivative along a single spatial dimension, the inverse current source density method inverts the electrostatic equations that map current sources at the recording sites onto recorded potentials. This matrix can then be used to solve the underlying CSD map. In constructing this matrix, spline smoothing was used to minimize spatial noise. Once the CSD had been calculated, its power spectrogram for each site was calculated and compared between sites recorded in the BLA versus those in adjacent structures.

Sleep-wake state detection was conducted in a semi-automated manner using EMG and EEG activity along with video motion detection.

2.11 Statistical analyses

All statistical tests were conducted using MATLAB. For IA performance, a two-way analysis of variance (ANOVA) was performed with Group (two levels) and Session (two levels) as independent variables. A two-way ANOVA was used because there is no non-parametric equivalent for multifactorial analyses. For HB performance, a Kruskal Wallis ANOVA was performed with normalized latency to the food reward as the independent variable. Unpaired *post-hoc* comparisons were performed using Fisher's Least Significance Difference (LSD), while paired comparisons were performed using the sign test. For average power changes between performance groups or types of modulation, a Kruskal Wallis ANOVA (for more than two levels), or a Mann Whitney test (for two levels) was conducted, with maximum power change as the independent variable. For assessment of the relationship between gamma power changes and performance, a Spearman's rank-

order correlation was performed. For individual burst treatment differences, a Kruskal Wallis ANOVA was performed on the incidence or amplitude change from baseline. For comparing MUA changes or phase locking changes, a Kruskal Wallis ANOVA was performed on percent firing rate changes or PPC changes relative to baseline for light-modulated cycles. Finally, for comparing sleep-wake state durations, a Mann Whitney test or a Kruskal Wallis ANOVA was performed on the percent time spent in each state between groups. All statistical tests were two-tailed, and significance was judged at the 0.05 level.

CHAPTER 3

Study of BLA-mPFC activity and interactions surrounding hippocampal DSs and SWRs during offline states

3.1 Background

The BLA mediates the facilitation of memory consolidation by emotion (McGaugh, 2004). It does this in part by influencing other brain areas involved in memory storage. One such area with which it has reciprocal connections is the mPFC. Previously, it was reported that mPFC gamma power and unit activity increases around hippocampal SWRs, which are thought to be important for the systems consolidation of memories (Remondes & Wilson, 2015). The BLA also exhibits gamma oscillations, particularly during emotional states. However, nothing is known about BLA oscillatory activity during SWRs. Thus, the present

study was undertaken to characterize BLA and mPFC activity in relation to SWRs and another population event generated by the hippocampus during NREM sleep, DSs.

3.2 Hypothesis

Since the BLA, mPFC and vHipp are interconnected, there should be a baseline level of communication, especially during offline states like quiet waking (QW) and NREM sleep, when BLA neurons are most active (Paré & Gaudreau, 1996) and the vHipp generates DSs and SWRs. Furthermore, previous results from our laboratory indicate that unit activity and gamma power in many cortical areas increase during NREM sleep in relation to DSs and SWRs (Headley et al., 2016). Thus, I hypothesize that BLA and mPFC unit activity and gamma power will increase in relation to the DSs and SWRs generated by the vHipp. To test this hypothesis, I obtained simultaneous unit and LFP recordings from the BLA, mPFC, and vHipp during offline states.

3.3 Materials and methods

Rats were implanted with electrodes in the BLA, mPFC and vHipp and spontaneous activity was recorded from these areas across multiple sleep-wake cycles. For technical details see sections 1,2,9,10,11 of Chapter 2.

3.4 Results

In total, 14 animals were implanted. Of them, 11 had successful implants in the BLA, 12 in mPFC, 10 in ventral CA1, and 8 in ventral DG. Spontaneous LFP and unit activity was recorded for several hours in a familiar environment. Analyses were restricted to QW and NREM, due to the higher incidence of DSs and SWRs in these periods (Buzsáki et al., 1992; Bragin et al., 1995a). DSs were identified by detecting positive peaks in the LFP that exceeded more than 5 standard deviations (SD) from the mean amplitude of the LFP recorded in the DG. SWRs were detected in a similar manner, but using trough detection at 2.5 SD in hippocampal LFPs. Below, DSs and SWRs recorded during QW and NREM epochs were combined.

Gamma power

Consistent with my hypothesis, the average spectrogram for DS-related BLA activity revealed an increase in gamma power, mostly in the 30-50 Hz range. This increase was centered around DS events, beginning 200 ms before and continuing up to 200 ms after the DS peak (**Fig. 3-1A**, **C;** 35,568 DSs from 5 animals). The same analysis for SWR-related BLA activity disclosed a more modest increase in gamma power, which peaked shortly after the SWR (~100 ms, **Fig. 3-1B**, **C;** 72,603 SWRs from 8 animals). The increase in BLA gamma (30-100 Hz) in relation to DSs was significantly higher than that associated with SWRs ($z = 1.94$, $p = .048$).

Similar results were obtained in the mPFC. That is, mPFC gamma power increased significantly more in relation to DSs (**Fig. 3-1D, F;** 71,539 DSs from 6 animals) than SWRs (**Fig. 3-1E, F;** 123,965 SWRs from 9 animals, z = 2.02, *p* = .042).

Overall, these results indicate that BLA and mPFC gamma power increases in relation to DSs and SWRs and that this effect is most pronounced in the low to mid-gamma range.

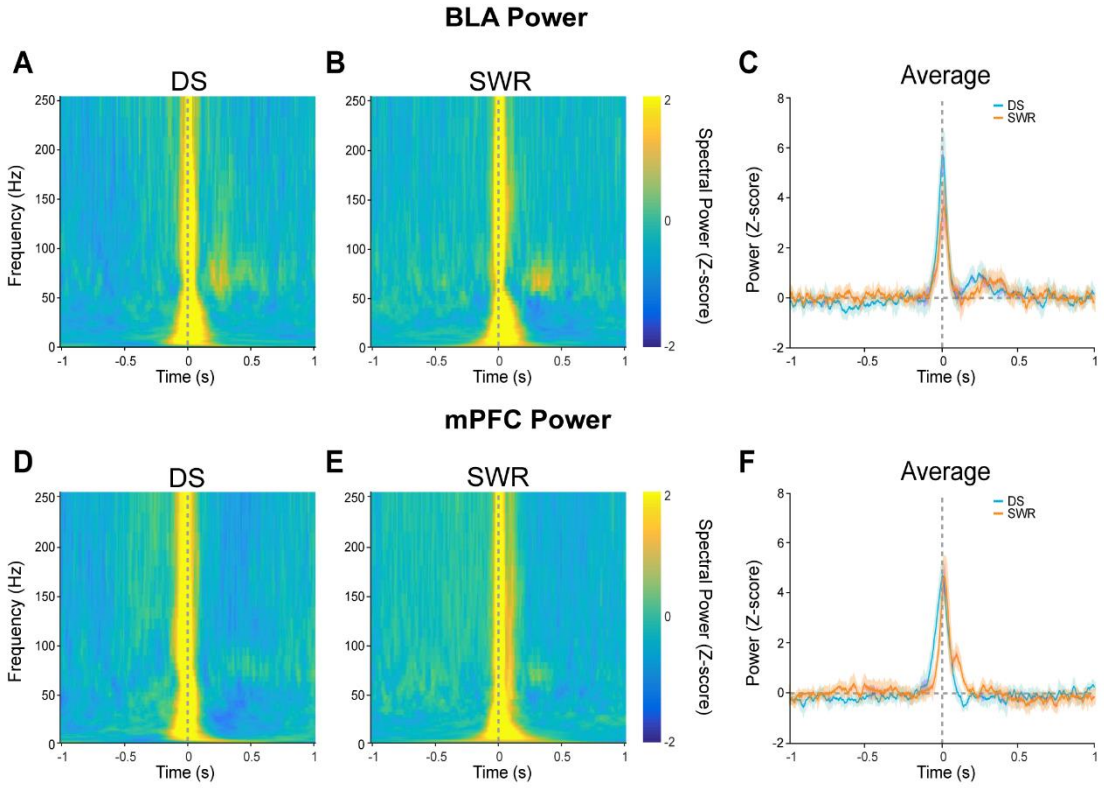

Figure 3-1: Average BLA (A, B) and mPFC (D, E) spectrograms surrounding DSs (A, D) and SWRs (B, E) during NREM and QW, as well as average gamma power comparison between events (C, F). Z-scores are calculated with a mean and standard deviation based on the activity 1 second before and after the peak of the events. Average power estimation is also in Z-scores.

Gamma coherence

Coherence between two areas can be evidence of communication between them, as stated in the CTC hypothesis (Fries, 2005). For this reason, coherence between BLA and mPFC was also studied around the same events. Indeed, BLA-mPFC gamma coherence increased in relation to DSs, paralleling the time course of the rise in gamma power. This effect was most pronounced in the 30-50 Hz range (**Fig. 3-2A**). In addition, coherence in the 60-80 Hz range increased starting 200 ms after DSs and lasting for 300 ms (**Fig. 3-2A**). In contrast, gamma coherence actually decreased during SWRs. This effect was followed by an increase in 50-90 Hz coherence, starting 100 ms after SWRs and nearly lasting for one second (**Fig. 3-2B**). Overall, gamma coherence between BLA and mPFC increases in relation to both DSs and SWRs, albeit with a different time course.

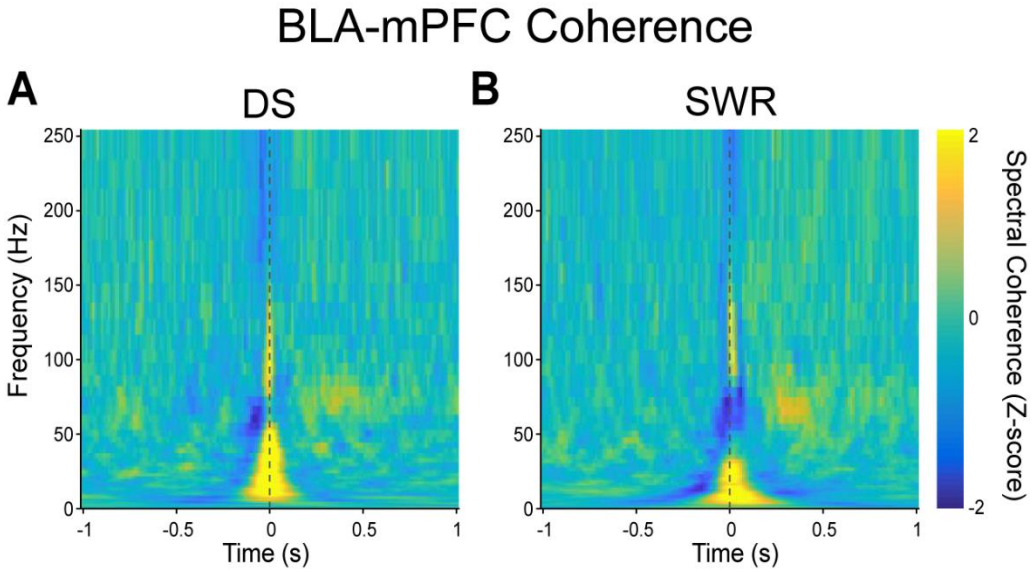

Figure 3-2: Average BLA-mPFC coherograms surrounding (A) DSs and (B) SWRs during NREM and QW. Z-scores are calculated with a mean and standard deviation based on the activity 1 second before and after the peak of the events.

DS- and SWR- related changes in unit activity

To further characterize BLA and mPFC activity during DSs and SWRs and rule out possible effects of volume conduction, single unit activity in the two areas was also studied. A total of 95 BLA and 106 mPFC units were recorded in 7 rats. Out of those, 24 BLA and 96 mPFC cells were analyzed during DSs, while 53 BLA and 96 mPFC cells were analyzed during SWRs. Peri-event histograms of unit activity were computed around DSs and SWRs, revealing that unit activity in both areas was indeed modulated by DSs and SWRs. For DSs, a similar proportion of modulated units were observed in BLA and mPFC (**Fig. 3-3A**, left). For BLA units, the largest modulation occurred ~100 ms prior to the DS peak, with most cells being excited (**Fig. 3-3A**, top right). In mPFC, an equal proportion of units were excited or inhibited. Generally, the maximal modulation occurred slightly before the DS peak (**Fig. 3-3A**, bottom right).

Moving on to SWRs, a similar proportion of modulated units was observed in the BLA and mPFC (Fig. 4B, left). Most BLA and mPFC cells were excited in relation to SWRs, with the largest modulation occurring ~10 ms after the peak (**Fig. 3-3B**, right).

In summary, our results indicate that DSs and SWRs modulate unit activity in the BLA and mPFC, with most cells showing maximal modulation before the peak of the DSs but after the peak of the SWRs.

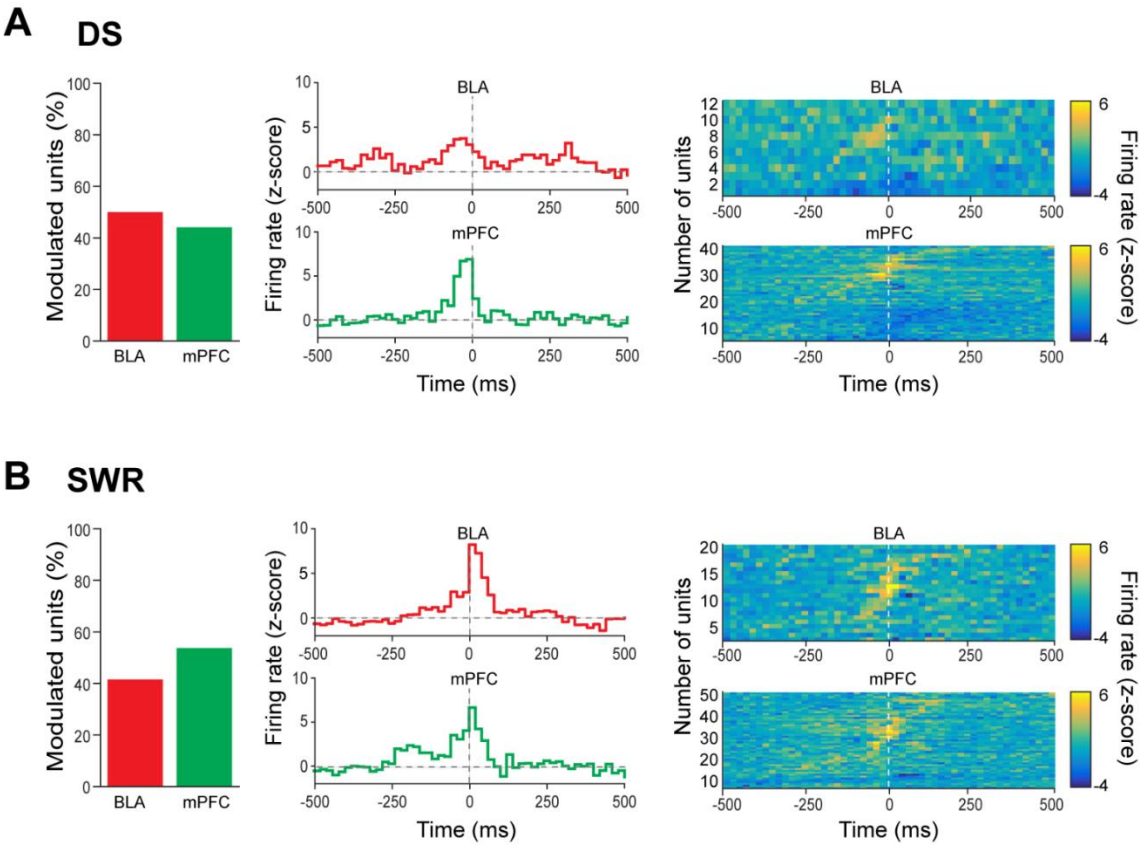

Figure 3-3: Single unit activity in the BLA and mPFC, as modulated by DS (A) and SWR (B). Percentage of single units modulated (left), examples of single unit PSTHs (center) and unit activity sorted by latency of peak modulation (right). Significance of modulation was assessed as two consecutive spike bins deviating more than 5 standard deviations from baseline, which was 2 seconds before and after the peak of the LFP event. Z-scores are calculated with a mean and standard deviation of the same baseline.

3.5 Conclusion

The results of this aim showed that gamma oscillations were present in both the BLA and mPFC during hippocampal SWRs and DS. Importantly, these oscillations were coherent between the two structures and this activation was accompanied by single unit modulation. These findings point to increased coordination between BLA and mPFC surrounding hippocampal population events during resting states. These interactions might participate in the modulation of systems consolidation by emotional arousal.

CHAPTER 4

Changes in BLA gamma band activity during the consolidation of an aversive memory

4.1 Background

Gamma oscillations in the BLA have been associated with the processing of emotional memories (Headley & Paré, 2013). Experimental evidence for their role comes from optogenetic manipulations of gamma activity in the BLA after inhibitory avoidance (IA) training, which boosts subsequent memory (Huff et al., 2013). Despite the importance of BLA activity for emotional memory consolidation, it remains unclear exactly what its spectral characteristics are following emotional experiences. The present study was undertaken to address this question.

4.2 Hypothesis

Since gamma oscillations are associated with emotional memory (Chapter 1.2), and post-training gamma band BLA stimulation can boost performance in IA (Huff et al., 2013), I expect that the BLA will show elevated gamma band activity during the post-training consolidation period of IA. To test these predictions, I recorded LFP activity in the BLA before and after IA training. I also tested recall of the IA memory during a retention test conducted 48 hours after training.

4.3 Materials and Methods

Implanted animals went through an IA protocol, and activity in the BLA was recorded before and after training. For technical details see sections 1,3,9,10,11 of Chapter 2.

4.4 Results

Inhibitory avoidance (IA) performance

During IA training, animals were placed in the light compartment of a light/dark box and, as soon as they entered the dark compartment, they received an inescapable 1 s/1 mA

shock. Two days later, retention was tested by placing the animals in the light compartment and measuring the time it took them to enter the dark compartment (**Fig. 4-1A**). Increased latency to enter the dark compartment compared to training indicates that the subject formed a memory of the aversive experience, whereas a similar or reduced latency indicates that it did not learn.

Analysis of individual performances revealed a wide range of latencies, with 7 subjects showing strong memory of the experience, while 6 subjects showed little to no memory (**Fig. 4-1B-C**, Good Learners and Poor Learners). Indeed, comparison of Training and Retention latencies in Good and Poor Learners showed significant main effects for both Group and IA training session, as well as a significant Group x Session interaction (**Fig. 4-1B**, $F(1,25) = 11.48$, $p = .0026$). Tukey's *post hoc* analysis indicated that Good Learners had a significantly increased Retention latency ($p = .0001$), whereas Poor Learners did not. Furthermore, Good Learners had a significantly higher Retention latency compared to Poor Learners ($p = .0001$), whereas their Training latencies did not differ. Thus, these results indicate that there are indeed two groups, showing either strong or absent memory of the aversive experience.

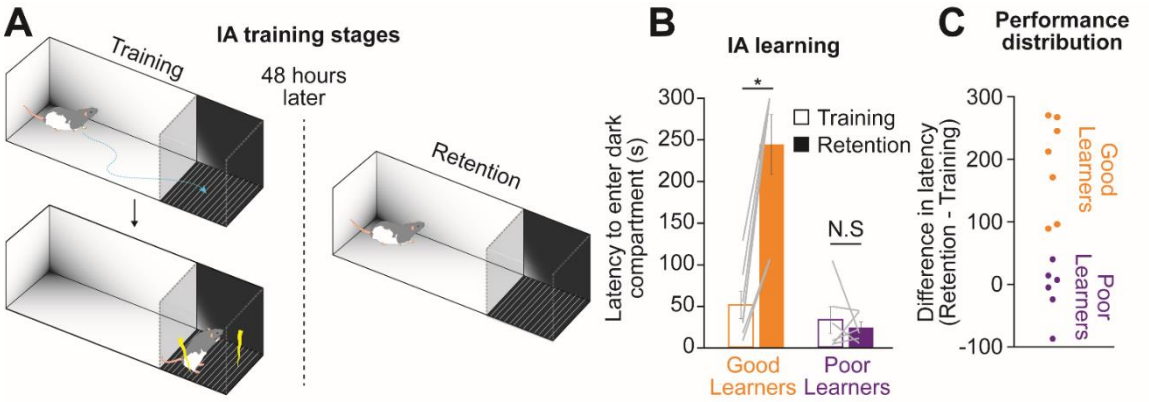

Figure 4-1: (A) Inhibitory avoidance (IA) apparatus and protocol. (B) Training and Retention latencies for both groups. Lines indicate individual subject performances. (C) Bimodal distribution of IA performance in Good and Poor Learners.

Gamma power

Local field potential activity was recorded from both groups of animals for a 1-hour period before and after IA training. BLA activity in Good Learners showed a pronounced post-training increase in mid-gamma band activity (40-60 Hz). This activity persisted for about 20 minutes after training (**Fig. 4-2A**, top). In contrast, Poor Learners showed less post-training increases in gamma activity (**Fig. 4-2A**, bottom). Comparison of spectral differences between the pre- and post-training phases revealed that mid-gamma power was increased only in Good Learners (**Fig. 4-2B**). Furthermore, consistent with the hypothesis that increased BLA gamma facilitates memory consolidation, there was a significant correlation between maximum gamma power change and retention latencies (**Fig. 4-2C**, $R = 0.66$, $p = .0171$). None of the spectral differences between groups were associated with differences in behavioral states seen after training (**Fig. 4-3;** Good Learners: n = 5 rats, Poor Learners: n = 5 rats; AW, Mann Whitney $U(9) = 28$, $p = 1$; QW, Mann Whitney $U(9) = 32$, $p = .42$; NREM, Mann Whitney $U(9) = 27$, $p = .94$).

4.5 Conclusion

In this aim, my experiments revealed increased gamma oscillations in the rat BLA during consolidation of aversive contextual memories. Furthermore, higher gamma levels correlated with better performance in inhibitory avoidance, pointing towards a role for BLA gamma oscillations in modulating consolidation strength.

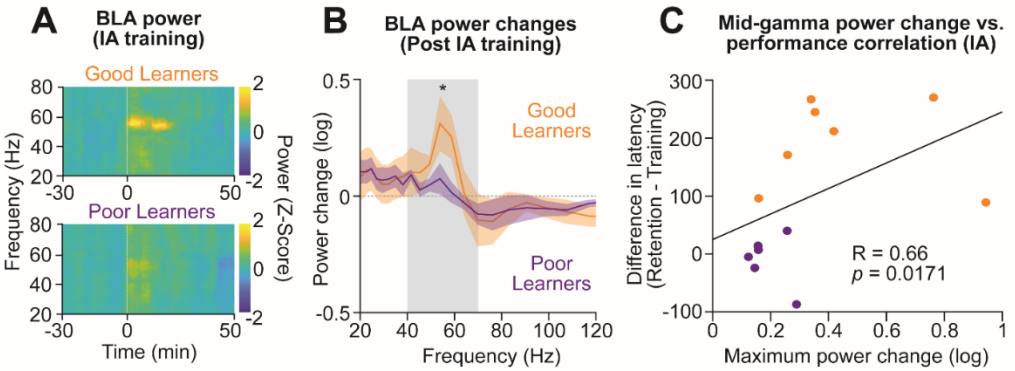

Figure 4-2: (A) BLA power spectrograms before and after IA training, for Good (top) and Poor (bottom) Learners. (B) Average power change (30 minutes Post-Training minus Pre-Training) for Good (orange) and Poor Learners (purple; Mann Whitney U(12)=66, p=.014). (C) Correlation between mid-gamma power change and IA performance (n=13 rats, Spearman's rank-order correlation R=0.66, p=.0171).

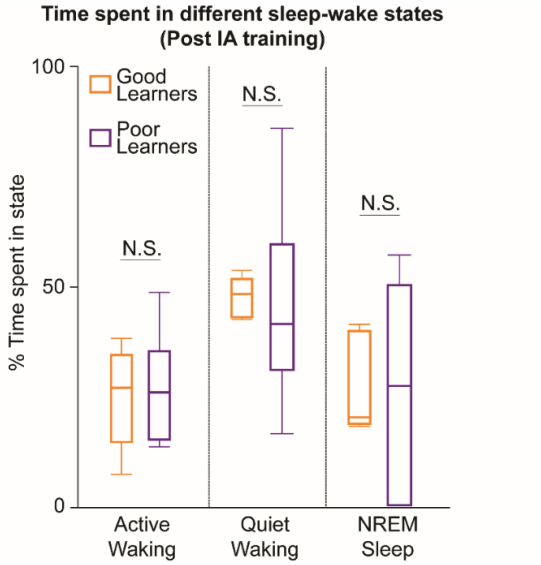

Figure 4-3: Percent time spent in Active Waking (AW, left), Quiet Waking (QW, center) and NREM sleep (NREM, right) for Good Learners (orange) and Poor Learners (purple).

CHAPTER 5

Changes in BLA gamma band activity during the consolidation of a positively motivated spatial memory

5.1 Background

BLA activity is not only linked to the consolidation of aversive memories, but also to positively motivated ones like the radial arm maze (Packard et al., 1994). In fact, the systems consolidation theory was mostly based on the study of spatial memory tasks (Morris, 1991). Therefore, there is reason to expect that similar mechanisms support the modulation of appetitive and aversive memories. However, this has not been directly tested yet.

5.2 Hypothesis

The results of Chapter 4 indicate that BLA gamma power is enhanced after training on an aversive task. Since BLA neurons are also activated during positively motivated tasks (Packard & Teather, 1998), it is likely gamma oscillations will arise there as well. Thus, my hypothesis is that the same changes in gamma power witnessed after IA will unfold after training on a positively motivated spatial memory task.

5.3 Materials and methods

I used a dry version of the Morris water maze called the Holeboard Task (Bast et al., 2005). In this task, rats form a spatial memory using allocentric cues in a single trial. Implanted animals were pre-trained and tested on the Holeboard task. Recordings were obtained before and after initial training, as well as after testing. For technical details see sections 1,4,9,10,11 of Chapter 2.

5.4 Results

Holeboard Task (HB) performance

Rats with restricted access to food were trained to retrieve a food pellet buried in one of 36 sand wells. Animals were first acclimated to the apparatus, and then trained to dig in the sand wells to retrieve food rewards. Once they became proficient at this, they were tested in the final version of the task. The animals had to use an allocentric strategy to memorize the location of the baited sand well (**Fig. 5-1A**). Various precautions were taken to make sure that the animals did not rely on proximal cues to solve the problem, such as mixing finely ground food inside all sand wells, using different start boxes on every trial, and rotating the apparatus while keeping the location of the baited well constant with respect to the distal cues.

The correct sand well location is acquired during the first trial where the food reward is visible, having been placed above the sand. Retention is tested in the three subsequent trials, which occur 1 hour after training (**Fig. 5-1B**). One of the three retention trials is a probe trial, in which the correct sand well is not baited. Whether the probe occurs in trials 3 or 4 is determined randomly, so that animals cannot predict when it will occur. The role of the probe trial is to assess task performance under conditions where it is impossible to use food odor-based strategies. Performance is measured across trials by the latency to approach the correct sand well.

Results show that the latency to approach the correct well significantly drops in retention trials (Trials 2-4, **Fig. 5-1C,** n=13 rats; Kruskal Wallis ANOVA, $\chi^2(4) = 82.05$, $p = 6.4 \times 10^{-17}$), while performance in probe trials is on par with that of baited trials (orange shaded box in **Fig. 5-1C**). Thus, animals are learning where the correct sand well is located solely using spatial cues. Furthermore, increasing the Training-Retention interval shows

that performance deteriorates with longer intervals (**Fig. 5-1D**). For this reason, a 1-hour interval was used in all subsequent recording experiments.

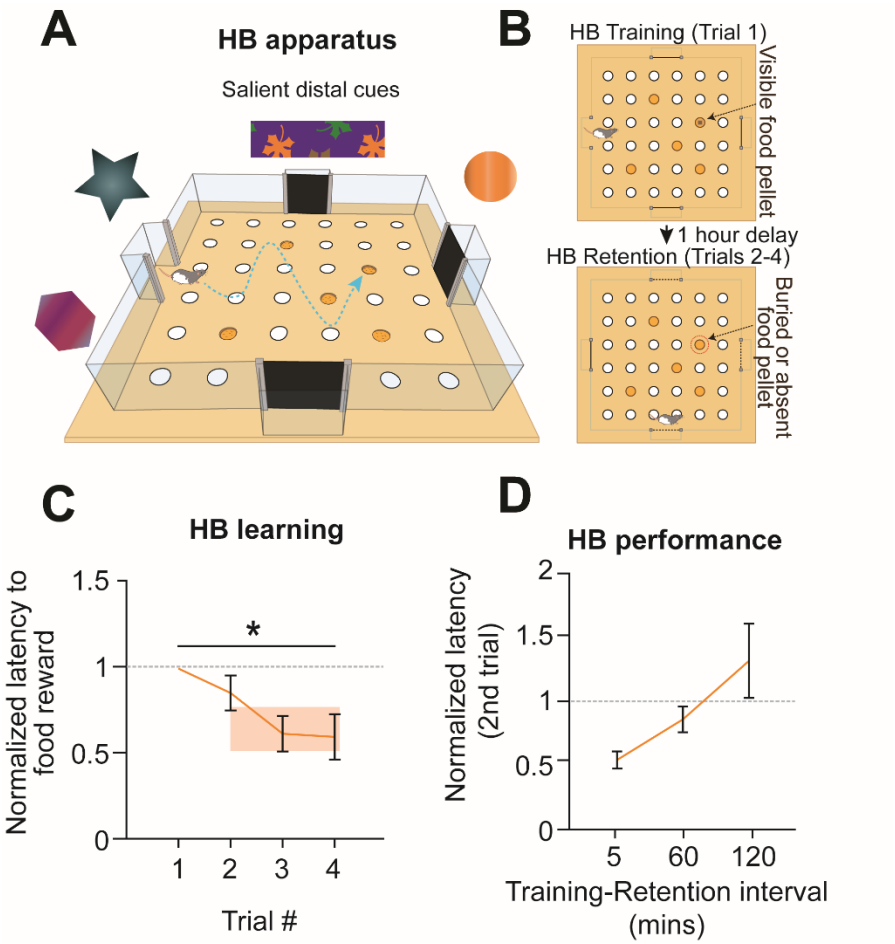

Figure 5-1: (A) HB Apparatus. (B) HB training stages. (C) Normalized latency to food reward across trials when Training-Retention interval is 60 mins. (D) Normalized 2nd trial latency for different Training-Retention intervals.

Gamma power

Local field potential recordings from the BLA of pre-trained animals showed an increase in mid-gamma power for approximately 20 minutes after training (**Fig. 5-2A,B**). This spectral change is similar to the one occurring after IA training (Power increase at 40-70 Hz; n = 49 sessions; 13 rats; Sign test $t(48) = 12$, $p = 4.88 \times 10^{-4}$), albeit weaker in amplitude. Furthermore, in this task the mid-gamma power changes are not correlated with performance (**Fig. 5-2C**, n = 13 rats; Spearman's rank-order correlation R = -0.16, p = .619).

A possible reason for the weaker mid-gamma changes seen in the HB task is the decreased salience of a food reward compared to unsignaled shock delivery. Furthermore, these recordings were performed in extensively trained animals, in contrast to the IA recordings which are performed in naïve animals. However, the spectral changes seen after both tasks are consistent in their frequency (**Fig. 5-3;** Kruskal Wallis ANOVA $\chi^2(2) = 0.22$, p = .986) and time course.

The BLA has neighboring cortical structures such as the piriform and perirhinal cortex that also exhibit gamma oscillations. To assess whether the gamma oscillations observed in the two learning tasks were generated in the BLA, two separate animals were implanted with multishank silicon probes. Recordings from these animals yielded sites in the BLA as well as adjacent structures such as the central amygdala (CeA) and striatum (STR). Current source density (CSD) analysis revealed that gamma oscillations were locally generated in BLA sites, whereas CeA and STR did not show the same result (**Fig. 5-4A,B**). Additionally, when looking at BLA sites stratified by their location on the dorsoventral

axis, gamma bursts occurred synchronously and with high phase coherence (**Fig. 5-4C,D**). Thus, gamma oscillations are generated in the BLA and are highly synchronous along its dorsoventral axis.

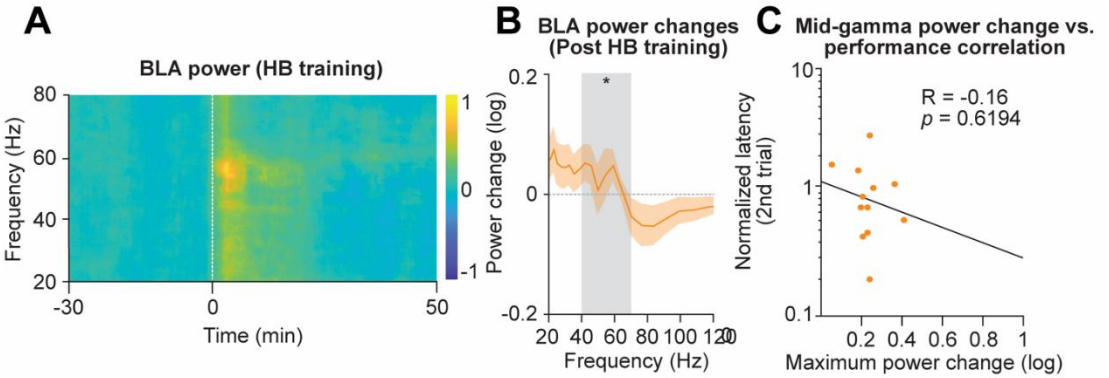

Figure 5-2: (A) BLA spectrogram before and after HB training. White dashed line indicates beginning of post-training recording. (B) Average power change post HB training. (C) Correlation between mid-gamma power change and HB performance.

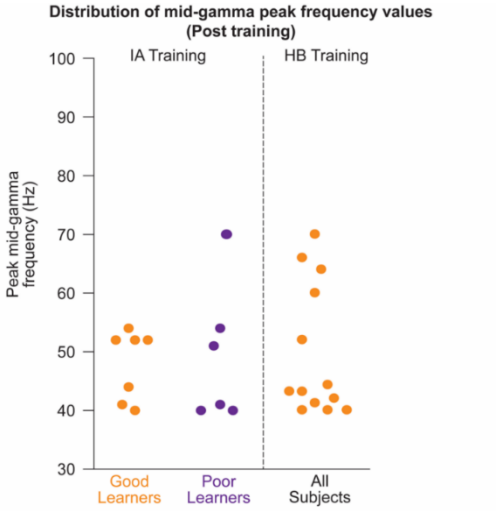

Figure 5-3: Mid-gamma frequency showing maximum power change post-training for IA (left, Good Learners: orange, n = 7 rats, Poor Learners: purple, n = 6 rats) and HB (right, All Subjects: orange, n = 13 rats). Horizontal offset for visualization purposes.

5.5 Conclusion

Gamma oscillations were boosted in the BLA after training in a positively motivated spatial learning task. These spectral changes were similar to the ones seen after aversive contextual learning, both in their frequency and duration. Furthermore, gamma oscillations were locally generated in the BLA and were highly synchronous throughout the nucleus. Overall, the timing of these changes in gamma power and their presence across learning tasks is in agreement with a possible role in the consolidation of emotional memories.

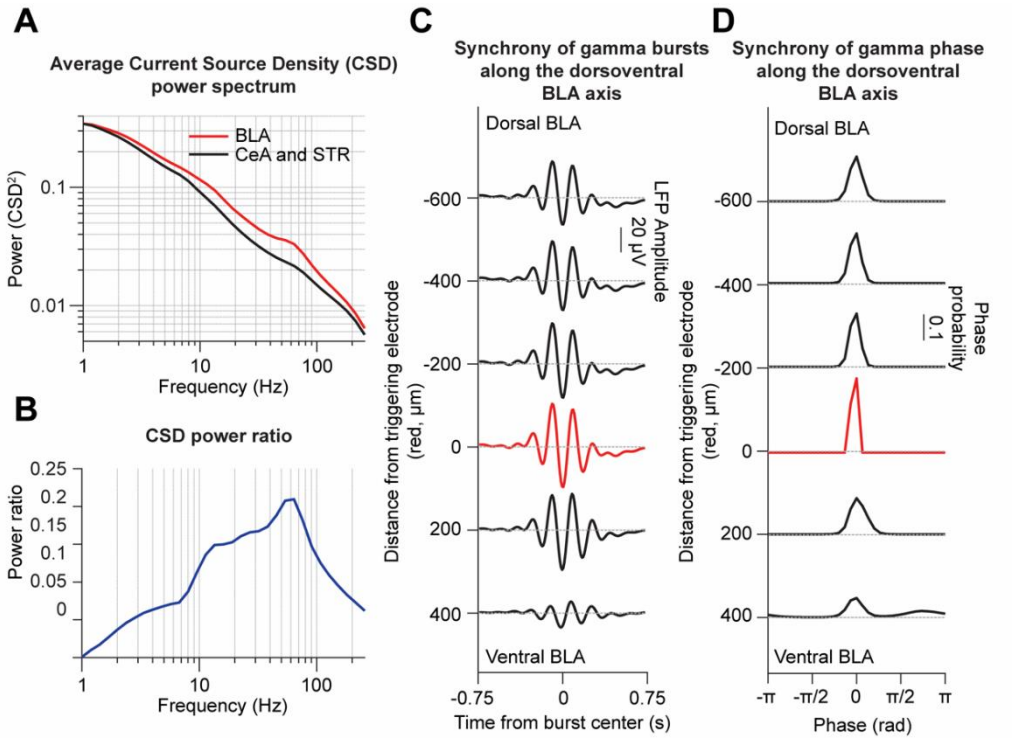

Figure 5-4: (A) Average Current Source Density (CSD) power spectrum for all BLA sites (red) and all CeA and STR sites (black). (B) Power ratio between BLA sites and outside sites. Ratio was calculated using the following equation: (Power in BLA sites – Power outside the BLA) / (Power in BLA sites + Power outside the BLA). (C) Average LFP in all dorsoventral BLA sites, triggered on gamma bursts occurring in red site. (D) Average phase probability distribution in all dorsoventral BLA sites, triggered on gamma bursts occurring in red site.

CHAPTER 6

Real-time control of gamma oscillations in the BLA

6.1 Background

It was reported that post-training optogenetic manipulations of BLA activity affect subsequent memory, with continuous stimulation at 40 Hz but not 20 Hz boosting memory and constant inhibition diminishing it (Huff et al., 2013). However, continuously stimulating the BLA at 40 Hz does not exactly reproduce the endogenous oscillations during consolidation. Gamma oscillations occur in short bursts and are coordinated with hippocampal activity (see Chapters 1 and 2). For this reason, real-time detection and manipulation of spontaneous gamma oscillations would provide a more precise test of the role of gamma in memory consolidation. However, real-time control of gamma oscillations in a frequency and phase specific manner has not been achieved yet.

6.2 Hypothesis

Gamma in the BLA occurs in brief bursts, with transient changes in excitability throughout the gamma cycle (Amir et al., 2018). For this reason, real-time tracking of gamma rhythms would provide the ability to modulate cells in line with their endogenous patterns. To overcome obstacles associated with tracking a fast rhythm in real time, I used programmable signal processors termed field programmable gate arrays. In contrast with conventional computer operating systems, which are continuously performing various tasks, FPGAs can perform signal processing in real time by instantiating dedicated circuits for specific computations. Taking advantage of this property, I implemented a custom-made algorithm that tracks the amplitude and phase of ongoing mid-gamma cycles with millisecond accuracy, allowing me to deliver brief optogenetic stimuli either in- or out-of-phase with network excitability, as indicated by the LFP.

6.3 Materials and methods

Animals received injections of an AAV5 driving the expression of Chronos, an opsin variant (Klapoetke et al., 2014), under a Synapsin promoter in the BLA (AAV5.hSyn.Chronos-GFP). Four to eight weeks later, they were implanted with optrodes and underwent a gamma modulation protocol during spontaneous activity. See sections 1,2,5-11 of Chapter 2.

6.4 Results

Gamma detection protocol and accuracy

In this custom-made algorithm, BLA LFPs are bandpass filtered at mid-gamma (40-70 Hz). When mid-gamma amplitude crosses a threshold and the algorithm detects a selected phase, a 2-ms light stimulus is delivered (**Fig. 6-1A**). To assess the accuracy of triggering, an artificial sinusoidal signal was passed through the algorithm (**Fig. 6-1B**). The system accurately detected the frequency and phase of the signal (**Fig. 6-1C-E**). Similar results were obtained when *in vivo* LFPs were used (**Fig. 6-1F,G**).

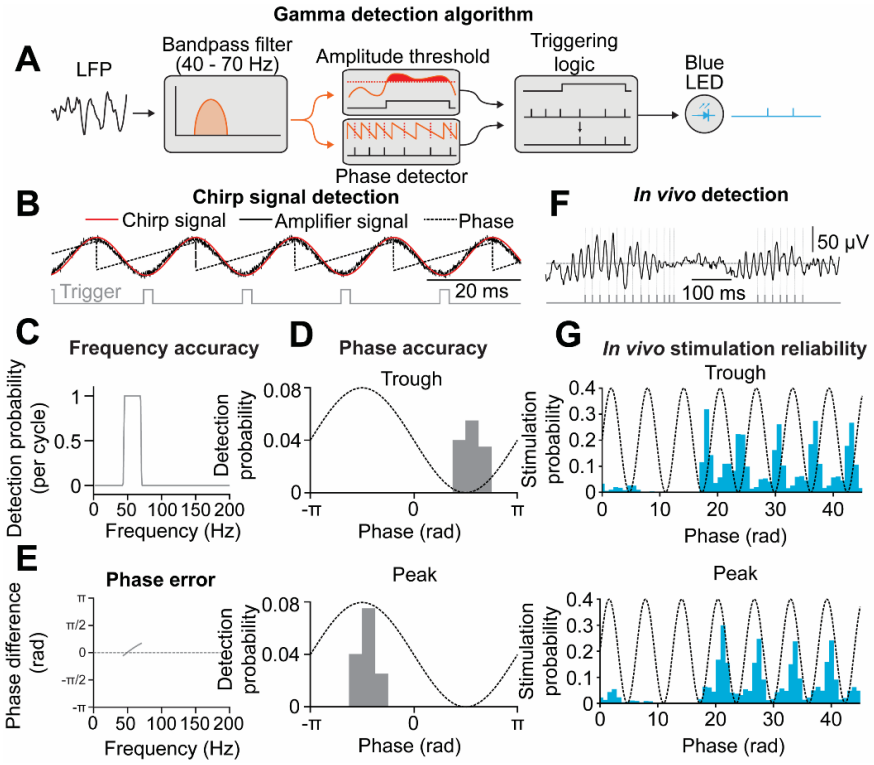

Figure 6-1: (A) Gamma detection method. (B) Example of trough detection (grey) on a chirp signal (red), amplified by our recording system (solid black). Dashed line: phase. (C) Chirp signal triggering probability across frequencies (selected band:40-70 Hz). (D) Phase detection error for same signal. (E) Triggering probability distribution for

trough (top) and peak detection (bottom). (F) Example of mid-gamma detection (grey) on LFP data. (G) *In vivo* stimulation reliability for trough (top) and peak (bottom, Trough: *n*=21 sessions, 8 rats, Peak: *n*=25 sessions, 9 rats).

BLA spectrograms during gamma detection show that pulses are preceded by bursts of mid-gamma power. The duration of mid-gamma bursts correlates with the number of pulses triggered (**Fig. 6-2**, top). Conversely, when pulses are randomly delivered, there is no consistent spectral change preceding them (**Fig. 6-2**, bottom).

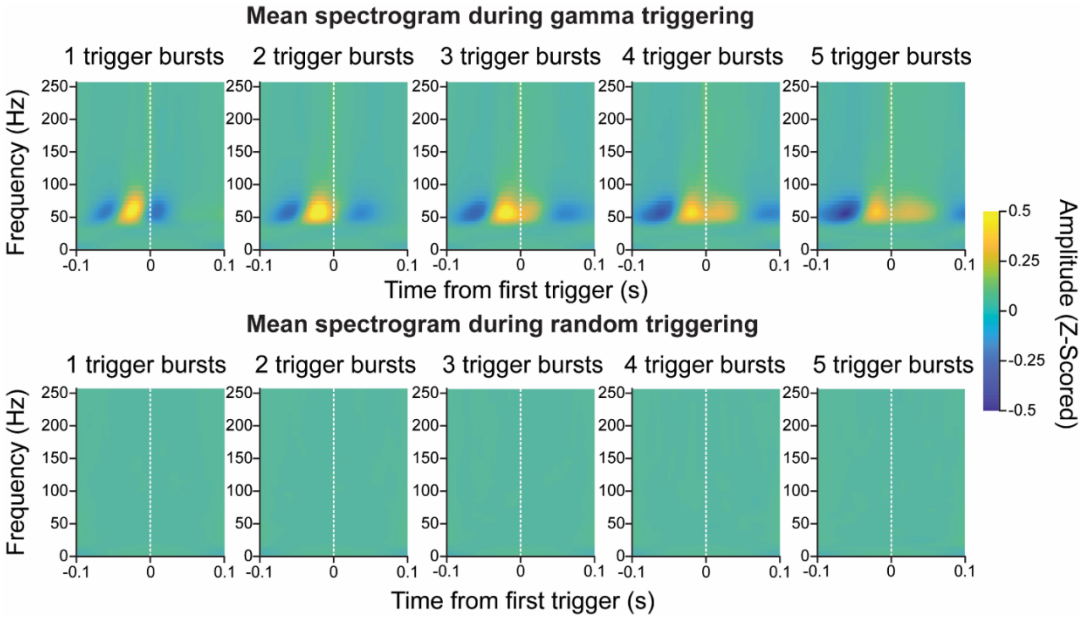

Figure 6-2: Average BLA spectrograms around the first trigger generated by the algorithm, for bursts containing different numbers of triggers (1-trigger to 5-trigger bursts, left to right). Top row: spectrograms during gamma detection. Bottom row: spectrograms during random triggering. Color bar: Z-scored spectral amplitude.

To further assess the accuracy of gamma detection, I calculated the probability of triggering based on the duration and the amplitude of a spectral burst for different bands, during gamma triggering or random triggering. For mid-gamma, triggering probability

increases with both longer duration and larger amplitude events (**Fig. 6-3B**). Underscoring the specificity of our triggering, other frequency bands, as well as random triggering, do not show the same result, but only the expected probability increase at long durations (**Fig. 6-3A,C,D-F**).

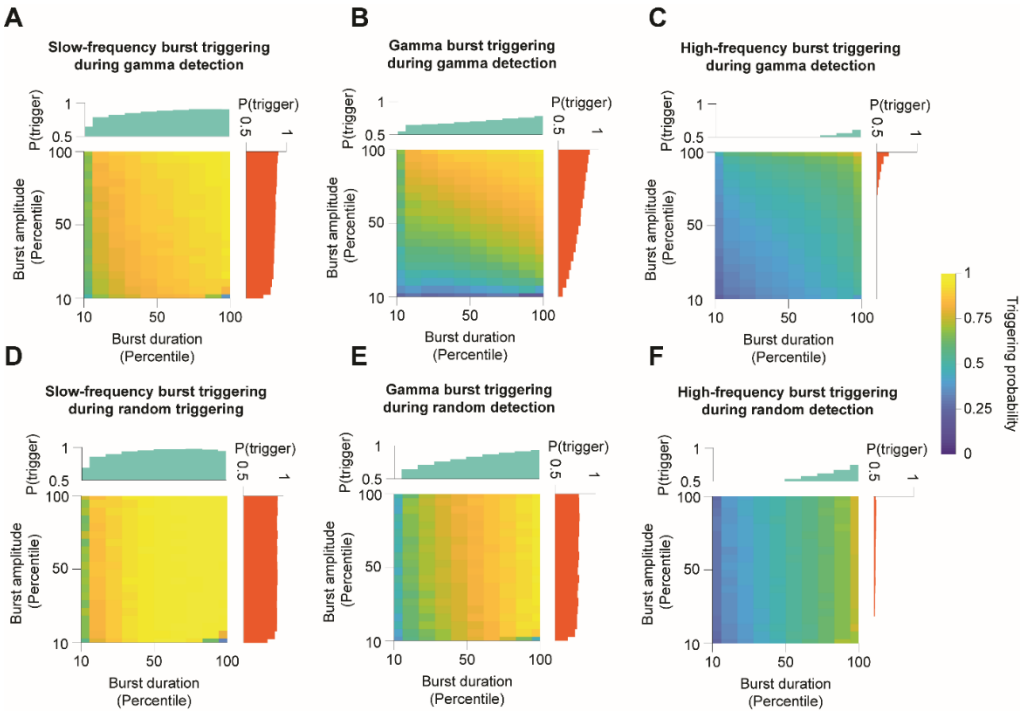

Figure 6-3: (A) Probability of triggering within slow-frequency bursts (1-30 Hz) during *mid-gamma detection*, stratified by slow-frequency burst duration (x-axis) and amplitude (y-axis). Side bar graphs indicate marginal distributions for the corresponding dimension. Color bar: Triggering probability. (B) Probability of triggering within mid-gamma frequency bursts (40-70 Hz) during *mid-gamma detection*. (C) Probability of triggering within high-frequency bursts (90-250 Hz) during *mid-gamma detection*. (D) Probability of triggering within slow-frequency bursts (1-30 Hz) during *random detection*. (E) Probability of triggering within mid-gamma frequency bursts (40-70 Hz) during *random detection*. (F) Probability of triggering within high-frequency bursts (90-250 Hz) during *random detection*.

In vitro validation of optogenetic approach

To maximize the method's temporal precision, I infected BLA neurons with Chronos (AAV5.hSyn.Chronos-GFP, **Fig. 6-4A**), a fast channelrhodopsin variant (Klapoetke et al., 2014), under the control of the ubiquitous Synapsin promoter. Surprisingly, *in vitro* whole-cell recordings of principal cells (PN) and fast-spiking (FS) interneurons (**Fig. 6-4B,C**) revealed that Chronos activation by blue light exerts prevalently inhibitory effects in the BLA. That is, light stimuli excited most FS cells (**Fig. 6-4D,E,H**), in turn eliciting picrotoxin-sensitive inhibitory potentials in PN cells (**Fig. 6-4F,G**). This tropism has been reported in the past in somatosensory cortex (Nathanson et al., 2009) and in this case was an advantageous result, since FS cells are particularly important for gamma generation (Sohal et al., 2009). *In vivo* recordings also indicated that the inhibitory interneuron network was recruited by optogenetic stimulation. 2-ms light pulses caused a transient increase of BLA multiunit activity (MUA) followed by a suppression (**Fig. 6-4I**). This coincided with an extracellular positive potential that lasted ~20 ms (**Fig. 6-4J**, blue). This potential likely reflected neural sources since it was abolished by isoflurane overdose (**Fig. 6-4J,** black; Mann Whitney $U(4) = 40$, $p = .0079$).

6.5 Conclusion

In this chapter, I tested the accuracy of a novel closed-loop optogenetic approach for tracking and modulating gamma oscillations in real time. The results show that the custom-made algorithm can reliably track gamma oscillations in both artificial and in vivo signals

with remarkable phase, frequency and amplitude accuracy. Furthermore, the optogenetic strategy used is appropriate for fast control of gamma oscillations.

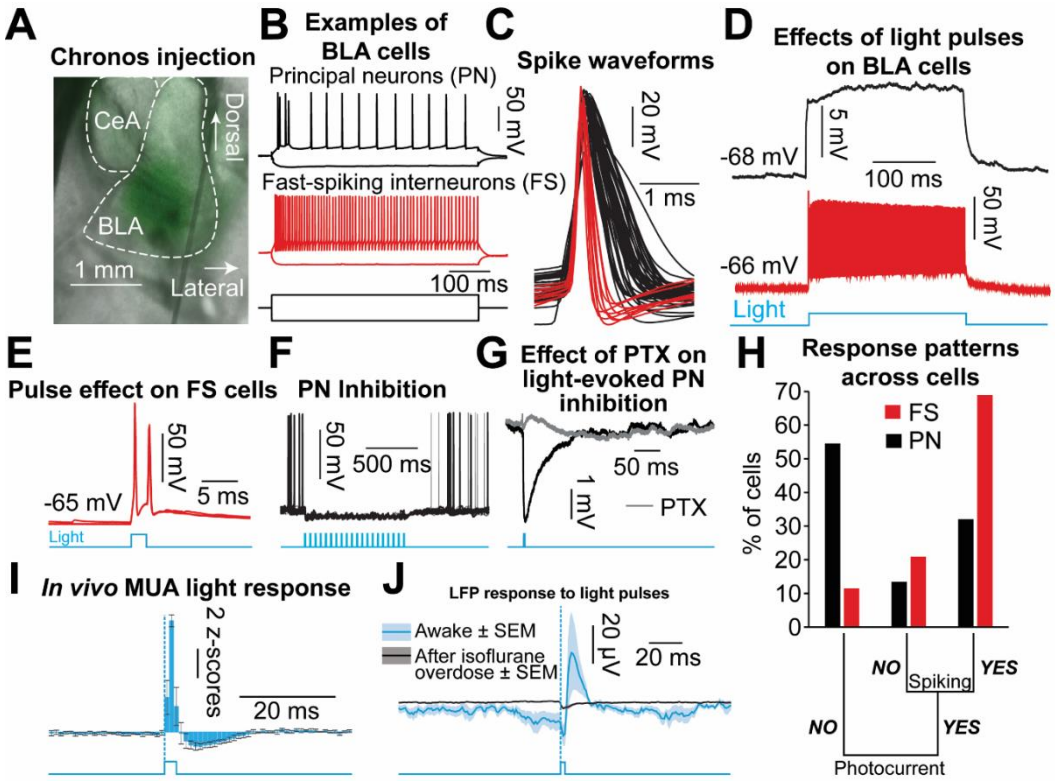

Figure 6-4: (A) Chronos injection (green) in the BLA. (B) Example recordings of BLA principal neurons (PN, black) and fast-spiking interneurons (FS, red). (C) Spike waveforms (*n*=53 cells, 10 rats). (D) Example responses to a 500-ms light pulse (blue). (E) FS responses to 2-ms light pulses (blue). (F) PN inhibition by a light-pulse train (blue). (G) Effect of picrotoxin (PTX-100 μM, grey) on light-evoked inhibition of PN (black). (H) Cell response patterns (PN-black, FS-red). (I) *In vivo* multiunit activity (MUA) response to 2-ms light pulses (*n*=6 sessions, 3 rats). Error bars: SEM. (J) Light-evoked LFP potential (average, blue±SEM, shading) by 2-ms pulses is abolished by isoflurane overdose (black, n=5 rats).

CHAPTER 7

Effects of closed-loop optogenetic modulation on gamma power and memory consolidation

7.1 Background

In Chapter 6 I described a novel closed-loop optogenetic approach for tracking and modulating gamma oscillations in real time. It was previously shown that interfering with BLA activity during the early stages of memory consolidation can affect subsequent retention of emotional experiences (McGaugh, 2004). Suggesting that gamma oscillations may play a role in this, stimulating the BLA at gamma frequencies enhances retention of aversive memories (Huff et al., 2013). Therefore, using closed-loop optogenetics in the BLA after training can potentially affect consolidation strength in a bidirectional manner.

7.2 Hypothesis

The new custom-made algorithm can detect troughs and peaks of gamma oscillations as they occur in real time. Fast-spiking interneurons show a preference for firing during the trough of gamma (Amir et al., 2018), whereas they are less active during the peak. Thus, stimulating in-phase with their excitation (Trough stimulation) might boost gamma oscillations and therefore increase consolidation strength. On the other hand, stimulating out-of-phase (Peak stimulation) will have the opposite effects.

7.3 Materials and methods

Animals received injections of an AAV5 driving the expression of Chronos, an opsin variant (Klapoetke et al., 2014), under a Synapsin promoter in the BLA (AAV5.hSyn.Chronos-GFP). Four to eight weeks later, they were implanted with optrodes and underwent multiple gamma modulation sessions after training in the HB task. See sections 1,2,5-11 of Chapter 2.

7.3 Results

Effects of closed-loop optogenetic modulation on gamma power

I modulated BLA mid-gamma for one hour after training in the HB task (between Trials 1 and 2). I chose this time window because consolidation of recently formed memories is particularly vulnerable to manipulations of neuronal activity performed in the first few hours after a new experience (Alvarez and Squire, 1994; Frankland and Bontempi, 2005; Wang and Morris, 2010). Moreover, the recordings indicated that this period also exhibited elevations in mid-gamma power (**Fig. 4-2A**). Virus-injected rats implanted with optrodes in the BLA (**Fig. 7-1**) were first placed in a familiar box ("home box") and recorded for 1 hour without stimulation (Light OFF; **Fig. 7-2A**). Mid-gamma triggering thresholds were determined during this period to achieve an average triggering rate of about 20 Hz (**Fig. 7-3A,B;** Light OFF: Kruskal Wallis ANOVA $\chi^2(3) = 0.53$, $p = .77$, Light ON: Kruskal Wallis ANOVA $\chi^2(3) = 4.49$, $p = .10$) and comparable inter-light pulse intervals across conditions (**Fig. 7-3C)**. Animals were then trained (Trial 1) and immediately placed back in the "home box" for 1 hour (Light ON; **Fig. 7-2A**), with one of four different treatments: light pulses were either delivered at the trough or peak of mid-gamma cycles (Trough and Peak treatments), at random times with respect to gamma (Random treatment), or during gamma, but with the light path blocked at the entrance to the implanted ferrule (Sham treatment), which controlled for sensory cues caused by light stimuli. Light intensity was adjusted to achieve an ~20 μV extracellular potential response and allow for adequate light spread

throughout the BLA (**Fig. 7-4**). After one hour of stimulation, animals were taken to the HB apparatus for retention testing (Trials 2-4; **Fig. 7-2A**).

Comparing the average gamma-band filtered BLA LFP around light pulses revealed that Trough treatment enhanced mid-gamma amplitude, whereas Peak diminished it (**Fig. 7-2B**). This was also evident in the spectrograms (**Fig. 7-2C;** Kruskal Wallis ANOVA, $\chi^2(3) = 32.05$, $p = 5.11 \times 10^{-7}$; Bonferroni corrected post hoc: Trough: p = 0.031, Peak: p = 0.029 and p=0.012 respectively) and power spectra reflecting the change between sessions (Light ON minus OFF; **Fig. 7-2D**). On the other hand, Random and Sham treatments had no significant effects on gamma power (**Fig. 7-2C,D**).

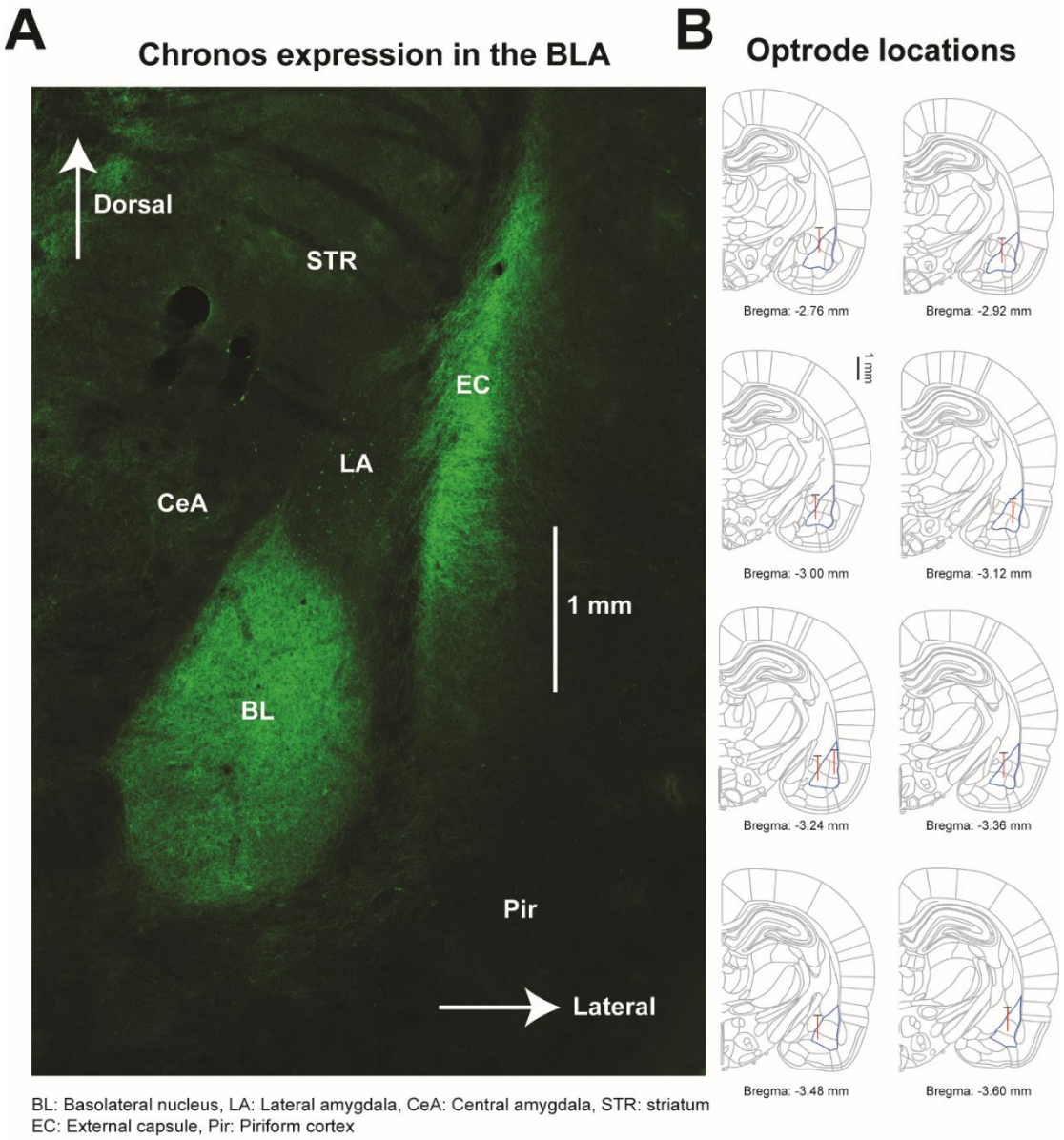

Figure 7-1: (A) Chronos expression localized in the BLA. (B) Electrode locations. Electrodes, red; fiber tips, horizontal black lines above the electrodes. BLA is outlined in blue.

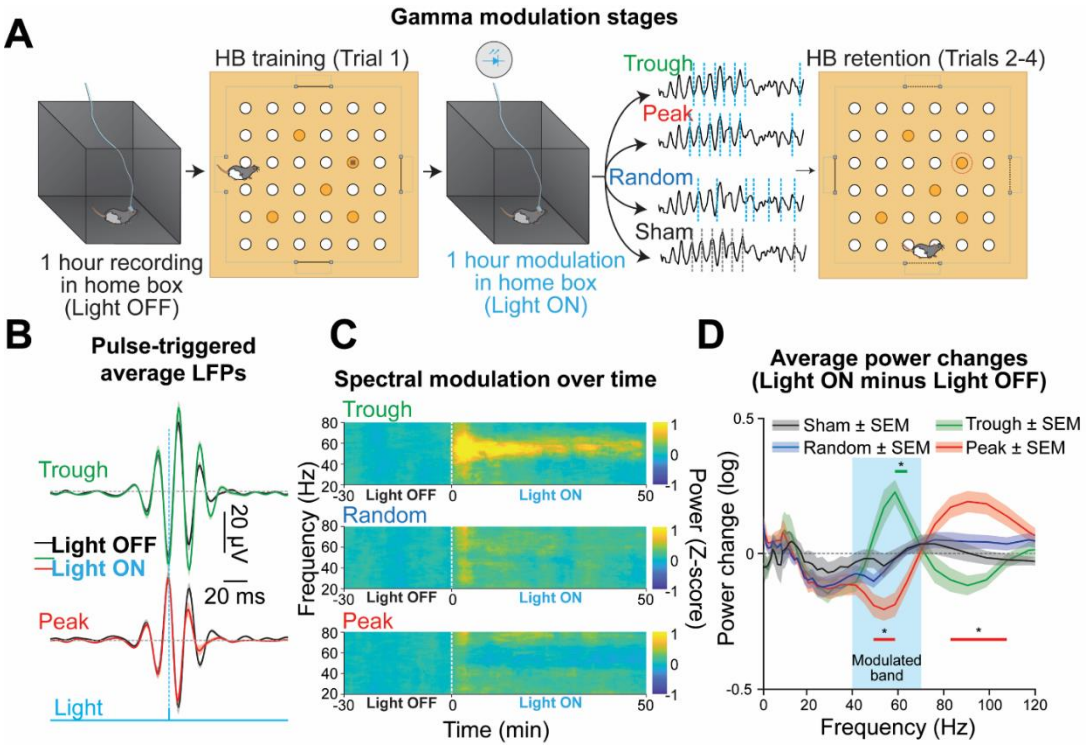

Figure 7-2: (A) HB training and modulation protocols. (B) Average filtered LFP around light pulses during Light OFF and ON. (C) BLA spectrograms for three modulation protocols. Dashed white line indicates Light ON start. (D) Average power changes (Light ON minus OFF). Blue rectangle outlines mid-gamma. Horizontal color lines indicate locations where a significant deviation from zero occurs per modulation condition.

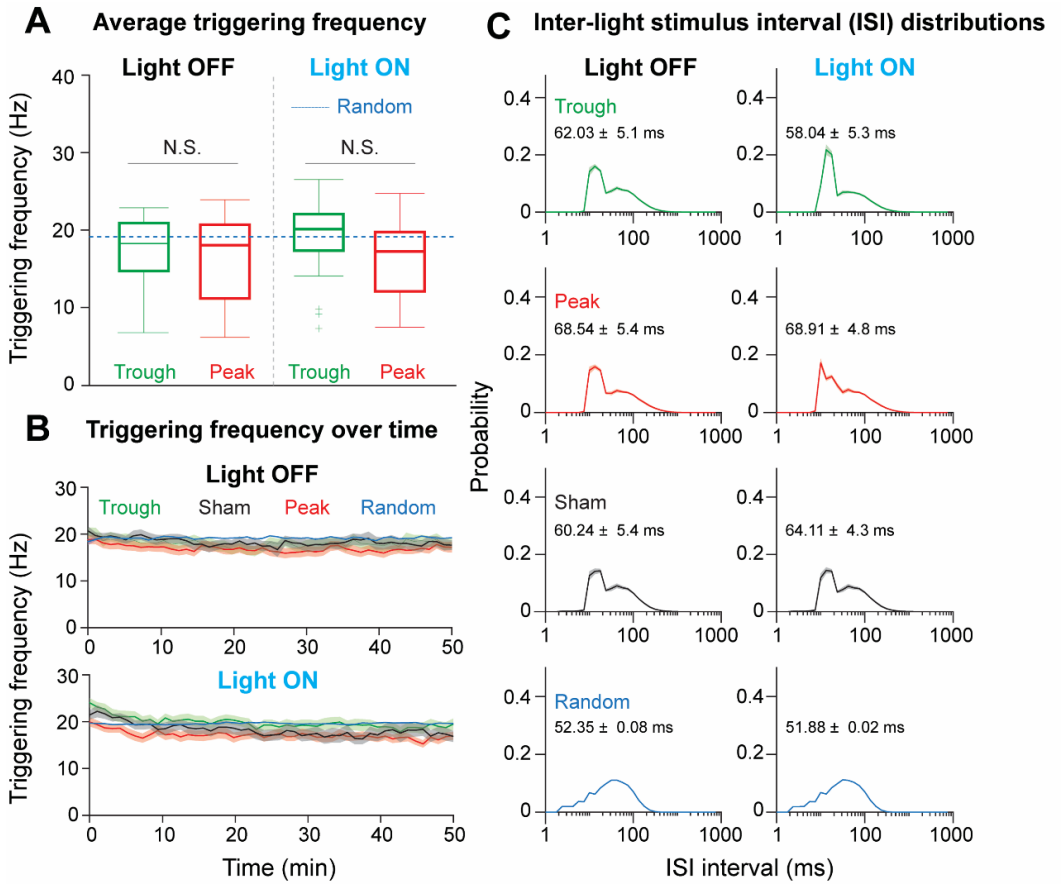

Figure 7-3: (A) Average triggering frequency for Light OFF (left) and Light ON (right) periods across treatments (Trough-green, Peak-red, Random-blue dashed line). Frequencies for Trough and Peak were determined by our threshold choice and gamma levels throughout the session. For Random, overall frequency was fixed at ~20 Hz. (Trough: *n* = 21 sessions, 8 rats, Peak: *n* = 25 sessions, 9 rats). (B) Triggering frequencies calculated per minute across the entire session for all treatments. Top: Light OFF, Bottom: Light ON. (C) Average inter-light stimulus interval (ISI) distributions for all treatments. Left column: Light OFF, Right column, Light ON. Numbers in each ISI histogram correspond to average ISI ± SEM for each treatment.

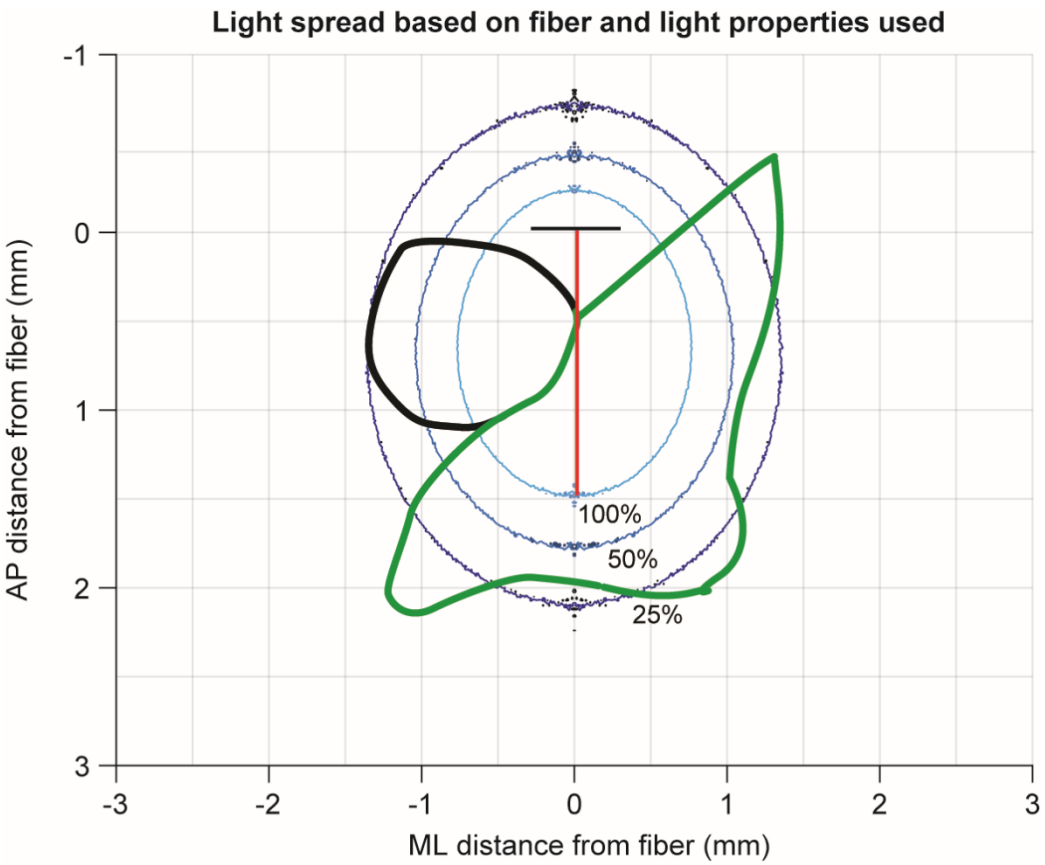

Figure 7-4: Estimated light spread based on the properties of our optic fibers (200 µm diameter, 0.39 NA) and light stimuli (465 nm wavelength, 2.6mW average power at fiber tip), using the model described in Stujenske et al., 2015. The contour lines reflect the amount of tissue that receives the corresponding percentage of our fiber tip power (100% - 0.24mW, 50% - 0.12mW, 25% - 0.06 mW). The black horizontal line marks the fiber tip and the red line is the protruding recording electrode in a representative animal. BLA: green, CeA: black.

Since gamma oscillations tend to occur as brief bursts, I examined the effects of our stimulation protocol at the level of individual mid-gamma bursts (**Fig. 7-5A**). Trough treatment increased the length (Kruskal Wallis ANOVA, $\chi^2(2) = 18.13$, $p = .0001$; Fisher's LSD post-hoc: Trough-Peak $p = .0003$, Trough-Random $p = .0001$, Peak-Random $p = .76$) and strength of gamma bursts, whereas Peak treatment only decreased burst amplitudes (**Fig. 7-5B,C;** Kruskal Wallis ANOVA, $\chi^2(2) = 9.33$, $p = .0094$; Fisher's LSD post-hoc: Trough-Peak $p = .0025$, Trough-Random $p = .26$, Peak-Random $p = .064$).

I next examined how gamma modulation affects multi-unit entrainment in the BLA. All treatment types where light pulses were delivered caused a minor (~20%) firing rate decrease (**Fig. 7-5F;** Kruskal Wallis ANOVA $\chi^2(2) = 0.41$, $p = .815$), consistent with the disproportionate recruitment of inhibition evident in our in vitro results (**Fig. 6-4B,C**). However, only Trough and Peak altered MUA phase locking to mid-gamma. Indeed, both treatments increased entrainment, but only when pulses were delivered during an individual burst (**Fig. 7-5D,E**; blue shading, Burst start: Kruskal Wallis ANOVA, $\chi^2(2) = 10.35$, $p = .0057$; Fisher's LSD post-hoc: Trough-Peak $p =. 26$, Trough-Random $p = .001$, Peak-Random $p = .034$. Burst end: Kruskal Wallis ANOVA, $\chi^2(2) = 9.02$, $p = .011$; Fisher's LSD post-hoc: Trough-Peak $p = .19$, Trough-Random $p = .003$, Peak-Random $p = .07$). Importantly, preferred phases differed between Trough and Peak treatment, with Trough augmenting entrainment to the preferred phase (Amir et al., 2018) and Peak shifting the preferred phase by ~90 degrees backward, thus making neurons fire earlier than expected in the gamma cycle (**Fig. 7-5G**).

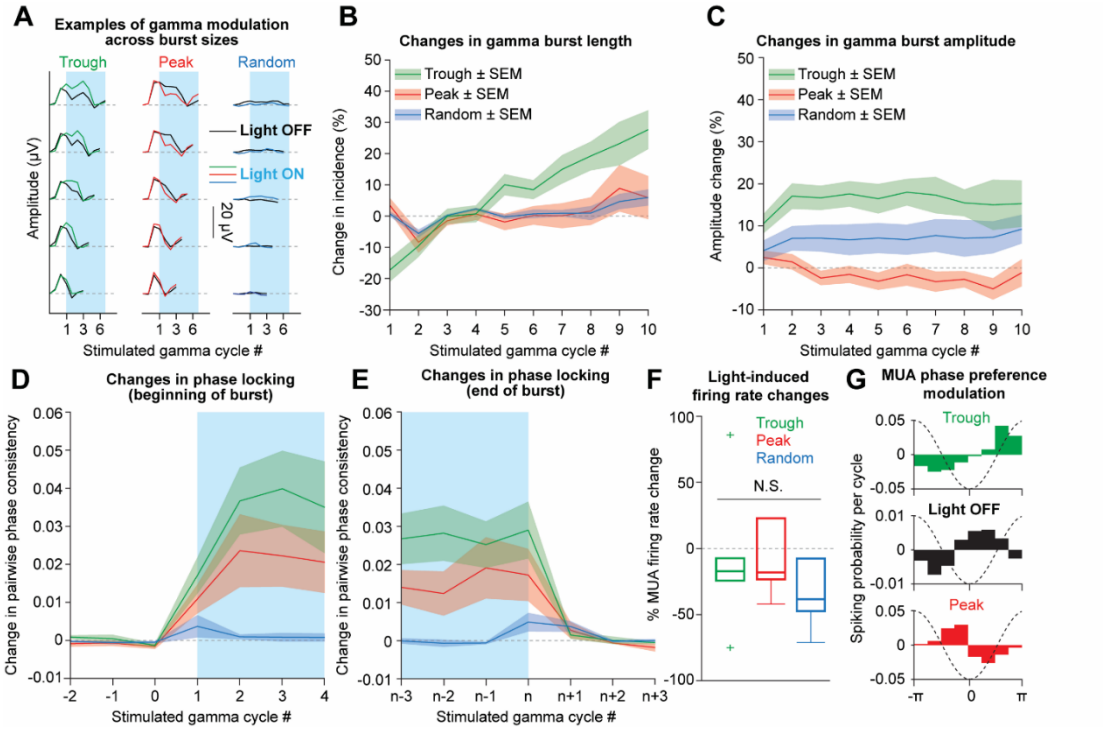

Figure 7-5: (A) Gamma amplitude examples across burst lengths (Light OFF-black, ON-colored). (B) Changes in burst length. (C) Burst amplitude changes. (D) Pairwise phase consistency (PPC) changes (Light ON minus OFF) before and after modulation starts in a gamma burst. (E) Same for modulation end. (F) MUA % firing rate change (Light ON – Light OFF/ Light OFF; Trough, *n* = 6 sessions, 3 rats; Peak, *n* = 6 sessions, 3 rats; Random, *n* = 6 sessions, 3 rats). (G) Phase preference (Green: Trough, Black: All Light OFF, Red: Peak).

Effects of closed-loop optogenetic modulation on behavior

Finally, I examined how modulating BLA gamma affects memory consolidation in the HB task by comparing latencies to the correct well as a function of treatment type (**Fig. 7-6A**). Note that no optogenetic stimulation was delivered during the retention phase. To assess mnemonic effects, we focused on the first retention trial (Trial 2), since every subsequent trial could depend in part on further training from the previous trial. For Trial 2, Trough treatment led to shorter latencies compared to Sham (**Fig. 7-6B**). In contrast, the Peak treatment impaired retrieval, whereas random light stimuli had insignificant effects (**Fig. 7-6B;** Kruskal Wallis ANOVA, $\chi^2(3) = 11.80$, $p = .0102$; Sign test *post-hoc*: Sham-Trough $p = .0391$, Sham-Peak $p =. 0391$, Sham-Random $p = 1$, Trough-Peak $p = .0039$, Trough-Random $p = .17$, Peak-Random $p = .0391$). These results were not due to treatment-related differences in sleep times (**Fig. 7-7A**) or distances to the baited wells (**Fig. 7-7B,C;** Kruskal Wallis ANOVA $\chi^2(3) = 3.24$, $p = .35$). Interestingly, our gamma modulation protocol altered the range of gamma levels present during the consolidation period. This unmasked a correlation between pre-to-post training changes in mid-gamma and performance in the HB task (**Fig. 7-6C;** Spearman's rank-order correlation $R = -0.63$, $p = .008$).

7.5 Conclusion

In this aim, I experimentally tested the functional importance of gamma changes during consolidation. To achieve this, I used the novel closed-loop optogenetic approach described in Chapter 6. By boosting or diminishing the post-training BLA gamma using this

algorithm, I bidirectionally modulated performance during a subsequent memory retention test. This suggests a causal relationship between BLA gamma and memory consolidation.

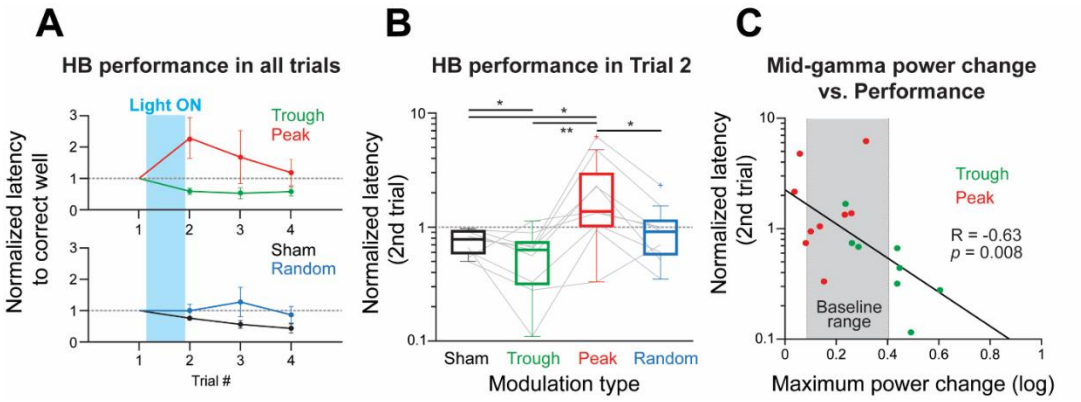

Figure 7-6: (A) Normalized performance on all HB trials, for experimental treatments (top) and control treatments (bottom). Light blue box shows modulation window (hour between the first and second trial - Light ON). Trial 1 to Trial 2: 1 hr ITI, Trial 2 to Trial 3: 5 min ITI, Trial 3 to Trial 4: 5 min ITI. (B) Normalized latency in the 2nd trial. Boxes show lower quartile, median and upper quartile; whiskers show the lowest and highest non-outlier observations. (C) Correlation between maximum mid-gamma power difference (Light ON minus Light OFF) and normalized 2nd trial latency for Peak (red) and Trough (green) sessions. Each dot is the average of all same trial types for one subject. Grey box indicates baseline range of values from Fig. 5-2C. Solid line: least squares fit.

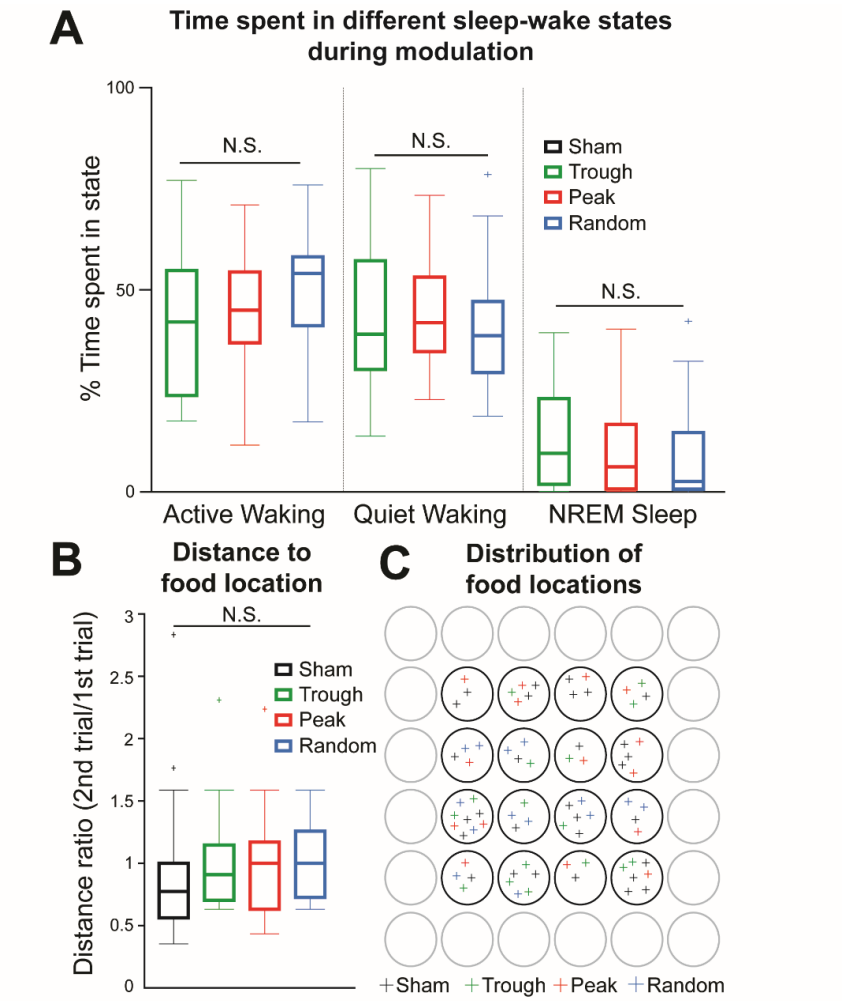

Figure 7-7: (A) Percent time spent in Active Waking (AW, left), Quiet Waking (QW, center) and NREM sleep (NREM, right); Trough-green (*n* = 21 sessions, 8 rats), Peak-red (*n* = 25 sessions, 9 rats), Random-blue (*n* = 22 sessions, 9 rats). (B) Ratio of linear distances between entry point and food location (2^{nd} trial distance/1^{st} trial distance. Sham-black (*n* = 30 configurations), Trough-green (*n* = 16 configurations), Peak-red (*n* = 15 configurations), Random-blue (*n* = 14 configurations)). (C) Distribution of food locations in all treatment sessions (Sham-black, Trough-green, Peak-red, Random-blue). Each cross represents the food location on a different maze configuration.

CHAPTER 8

Discussion

8.1 Overview

The experiments performed in this dissertation investigated how the amygdala facilitates the consolidation of memories for emotionally arousing experiences. The results clearly support the role of gamma oscillations in this process. First, gamma oscillations were shown to facilitate interactions between consolidation-related regions during sleep. Furthermore, gamma rhythms were present in the amygdala during the consolidation of emotional experiences, irrespective of their valence. Finally, using a new approach to control gamma rhythms in real time, I directly tested the importance of gamma in memory consolidation. In the following sections, I will discuss the findings of each experiment and their significance for memory consolidation.

8.2 Gamma oscillations increase BLA-mPFC-vHipp communication during offline states

In the experiments of Chapter 3, I found that during offline states, BLA and mPFC showed enhanced gamma power and unit activity in relation to DSs and SWRs. Furthermore, there was a concurrent elevation in gamma band coherence between the two areas, which suggests that mPFC-BLA interactions are facilitated during DSs and SWRs. Indeed, gamma oscillations are thought to promote interregional communication (Fries et al., 2015), as discussed in Chapter 1. Furthermore, mid- to high gamma oscillations entrain BLA unit activity more strongly than lower frequency oscillations (Amir et al., 2018). Given the reciprocal connections between the BLA and mPFC, the timing of the firing rate changes seen related to DSs and SWRs supports the following models of interactions during offline states (**Fig. 8-1**).

Shortly before DSs, BLA and mPFC show increased gamma interactions, which lead to a coordinated activation of dentate granule cells. This effect is most likely mediated via the rhinal cortices, which receive mPFC and BLA inputs. The activation of dentate granule cells causes hilar interneurons to discharge, triggering a DS event (**Fig. 8-1A**). This model is supported by the current finding that increases in BLA and mPFC gamma power and coherence as well as unit activity occur almost simultaneously with DSs. I also observed a rise in BLA-mPFC gamma coherence following DSs, which might have resulted from the downstream effects of DSs, likely through CA3 and CA1.

During SWRs, the synchronized firing of CA1 pyramidal cells activates the mPFC and BLA. This results in elevated gamma power and unit activity immediately following SWRs. While this initial co-activation is uncoordinated, over several hundred milliseconds the reciprocal connections between mPFC and BLA enable them to synchronize and exhibit increased gamma coherence. (**Fig. 8-1B**). These results agree with the timing of the increased gamma coherence and unit activity right after SWRs.

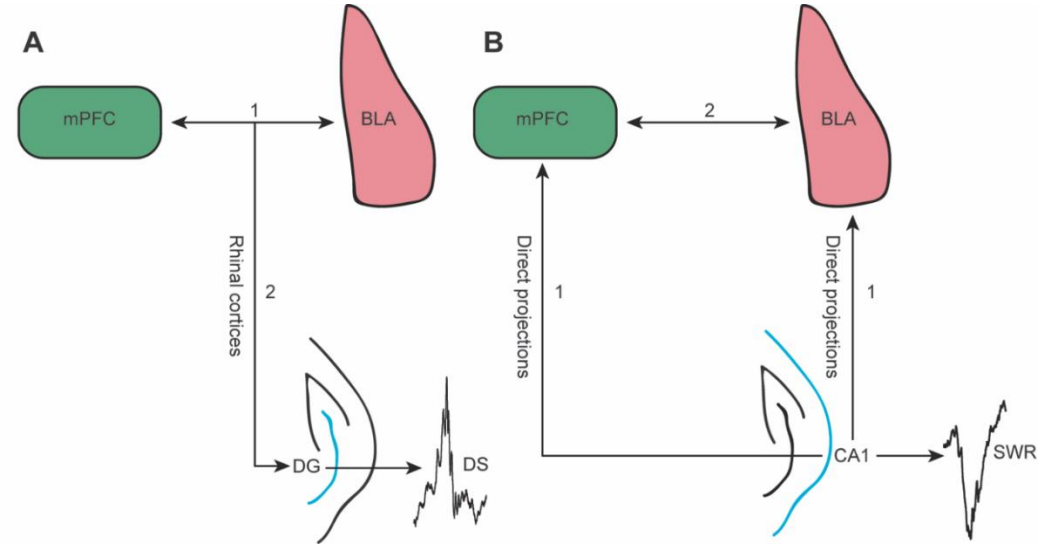

Figure 8-1: Hypothetical model of interactions between the mPFC, BLA and hippocampus in relation to DSs (A) and SWRs (B). Numbers and arrows indicate order of events and directionality of communication.

Both models illustrate how coordinated interactions between the mPFC, BLA and hippocampal formation are orchestrated around SWRs and DS. Given the importance of these structures in memory, these concentrated bouts of communication may be especially important for systems consolidation. In fact, gamma oscillations appear during hippocampal population events across many neocortical areas (Headley et al., 2016). Since oscillatory synchrony is important for effective interregional interactions (Fries et al.,

2015), it is not surprising that multiple areas would show coherent gamma band activity during offline states, something that has already been observed for slower rhythms (Molle et al., 2001; Colgin, 2011). The timing of these gamma interactions during hippocampal population events further supports their importance for memory consolidation, since DSs and SWRs already have an established role in that process (Lensu et al., 2018; Todorova & Zugaro, 2018). Thus, the effects of emotional arousal on consolidation may depend on a transient communication increase between the amygdala and neocortical structures, paced by hippocampal events during sleep.

8.3 Gamma oscillations are boosted during the consolidation of emotional memories

After IA training, I observed a rise in BLA mid-gamma that lasted for at least 15 minutes (Chapter 4). Moreover, this change in gamma power positively correlated with retention of the aversive memory. Importantly, these spectral changes are valence-independent, since a similar increase was observed after training in a positively motivated spatial learning task (Chapter 5). While the spectral changes are less pronounced in the HB task, this is expected because foraging for food in a familiar environment is far less arousing than receiving an unsignaled footshock. Furthermore, no correlation was present between post-training gamma power and retention in the HB task without light stimulation. This may be due in part to the narrower range of changes in gamma power elicited by the HB compared with the IA task.

Overall, it is important to note that in both tasks, we observed a boost in gamma power at the same time during consolidation, and in a similar frequency band. The relevance of these common activity patterns is supported by previous findings showing that inactivating the BLA in the first thirty minutes after training can affect both appetitive and aversive memories (Packard et al., 1994; McGaugh, 2004).

The increase in BLA gamma power seen post-IA in Good Learners is consistent with prior results, in which post-training gamma band stimulation of the BLA enhanced subsequent IA retention (Huff et al., 2013). In addition, a few studies have shown that gamma coherence between the BLA and other structures during conditioning predicts subsequent memory strength (Bauer et al., 2007; Popescu et al., 2009). This indicates that BLA gamma activity during both training and consolidation might be enhancing permanent memory storage.

How would this sustained increase in BLA gamma support systems consolidation? As Chapter 3 showed, there is elevated gamma communication between the BLA and mPFC during hippocampal SWRs. These population events have a known role in memory, as evidenced by their increased occurrence during early consolidation, among other findings (Todorova & Zugaro, 2018). Thus, the spectral changes seen in the BLA after emotional learning co-occur with an increase in SWR rate and the accompanying modulation of BLA-mPFC coherence. The importance of these multi-way interactions will be discussed in more detail in a later section (Chapter 8.4).

8.4 A novel closed-loop method for modulating gamma oscillations in real time

The experiments described in Chapters 3-5 revealed that gamma oscillations are enhanced in the BLA following an emotionally arousing experience, and that the strength of this enhancement correlates with subsequent memory. However, these results by themselves cannot establish a causal link between gamma oscillations and consolidation.

Prior to this study, much correlative evidence implicated gamma oscillations in various cognitive processes. Gamma rhythms appear in multiple studies during learning (Bass and Manns, 2015; Popescu et al., 2009; Stujenske et al., 2014), while stimulation at gamma frequencies enhances performance in various tasks (Huff et al., 2013; Cardin et al., 2009). However, due to technical limitations, prior optogenetic studies used fixed stimulation routines to upregulate gamma (Atallah and Scanziani, 2009; Cardin et al., 2009; Huff et al., 2013; Ni et al., 2016; Siegle et al., 2014), without taking into account the transient, "bursty" nature of this rhythm, as well as its variations in frequency (Colgin et al., 2009). Indeed, the transient nature of gamma bursts may reflect discrete periods of information processing (Lundqvist et al., 2016; Palmigiano et al., 2017). Thus, tonically altering gamma may force the network into an abnormal state (Jazayeri and Afraz, 2017). Furthermore, previous experiments could not account for non-specific effects, such as overall changes in neuronal excitability. Lastly, no studies tested the effects of specifically downregulating gamma oscillations and thus could not causally link gamma to specific behaviors and cognitive processes. Thus, there was a need to track the occurrence of individual gamma bursts in real time and achieve full control over these brief variations in intrinsic excitability patterns to directly test their role.

The best way to overcome these technical limitations is to use closed-loop signal processing combined with optogenetics. In closed-loop systems, the LFP signal is

processed in real time and its momentary state is assessed to control delivery of optogenetic pulses (Grosenick et al., 2015). However, previous approaches based on closed-loop optogenetics *in vivo* were only applied to slow oscillations (Siegle & Wilson, 2014; Dejean et al., 2016), while the only study performing closed-loop phase-locked tracking of fast rhythms was recently done *in vitro* (Nicholson et al., 2018).

Prior computer-based closed-loop studies were limited to oscillations of low frequencies, because conventional computer operating systems continuously perform various maintenance tasks that are unrelated to signal processing and take up a significant portion of their available resources. Thus, real-time processing on desktop computers running conventional operating systems is restricted to slow events. In Chapter 6, I describe a novel approach that allows rapid closed-loop signal processing with minimal delays, using separate programmable processors named FPGAs. FPGAs only perform the computations required for real-time signal processing, therefore minimizing time lags and allowing nearly instantaneous output. Importantly, custom-made scripts can be used to program these circuits according to our experimental needs.

The custom-made algorithm used here could reliably track the frequency, phase, and amplitude of *in vivo* mid-gamma bursts as they occurred in real time. A previous study from our laboratory had shown that BLA principal cells and fast-spiking interneurons increased excitability during specific phases of the gamma cycle. Both cell types show increased firing during the trough of the cycle. On the other hand, they have a relatively low preference for the peak (Amir et al., 2018). Stimulating BLA cells in- or out-of-phase with their excitability patterns could in theory lead to bidirectional control over the strength

of the rhythm (Hasenstaub et al., 2005). Therefore, the algorithm was programmed to track the occurrence of mid-gamma troughs or peaks.

For the question at hand, based on the findings from Chapters 3-4, I focused on detecting mid-gamma bursts. However, the algorithm can be used to study other rhythms, by simply adjusting the filters used (see Chapter 2.7). Given the variety of cognitive functions that gamma oscillations are thought to support, as well as the widespread presence of other oscillatory rhythms throughout the brain, the present study introduces a versatile method with many potential applications in neuroscience research.

8.5 Closed-loop bidirectional control of gamma oscillations modulates memory consolidation strength

In Chapter 7, I show that this closed-loop optogenetic method bidirectionally modulates the strength of BLA mid-gamma oscillations immediately after training in the HB task. Furthermore, the changes are frequency-specific, occur at the individual burst level and are accompanied by effects on multiunit entrainment. Importantly, by boosting or diminishing BLA gamma strength post-training, I witnessed bidirectional effects on the rats' retention during a subsequent memory test. This suggests a causal relationship between BLA gamma and memory consolidation.

Spectral results agreed with the hypothesis that gamma oscillations are boosted when cells are optogenetically activated in-phase with their intrinsic excitability patterns

(Trough), while the opposite effect was observed for out-of-phase stimulation (Peak). There are two possible ways through which in-phase closed-loop stimulation can affect BLA cell entrainment to gamma: first, cells that are already phase-locked to gamma might fire more at the preferred phase, thus increasing the amount of entrainment to gamma; second, cells that are not already phase-locked might start showing entrainment, therefore increasing the number of cells participating in the rhythm. In both cases, this is being reflected as a net increase in mid-gamma spectral power, as well as an enhancement of multiunit entrainment, as seen in Chapter 7. Surprisingly, out-of-phase stimulation of BLA cells was also shown to enhance entrainment, but at the opposite phase compared to baseline conditions. Presumably, this alters interactions between principal cells and interneurons during the gamma cycle, therefore leading to the observed suppression in gamma strength.

These bidirectional effects on gamma power after learning led to pronounced differences in consolidation strength, as evidenced by performance during retention. Specifically, the stronger the gamma levels during consolidation, the faster the animal would retrieve the hidden food reward, indicating improved spatial memory. Due to the nature of the HB task, I had the ability to train the same animal on multiple sessions by changing the configuration of the maze. Thus, I could perform within-subject comparisons of the behavioral effects caused by various gamma modulation protocols. This allowed me to show that the same animal exhibited significant differences in retention levels depending on the type of modulation used during consolidation.

Critically, these findings highlight the importance of delivering light stimuli at specific phases of the endogenous gamma rhythm. These experiments were designed to

overcome previous limitations and control for confounding factors, since the only parameter that changed between experimental conditions was the precise timing of light delivery with respect to the ongoing gamma phase. Yet, this very slight temporal difference (~7 ms on average) between conditions resulted in opposite effects on gamma levels and behavior.

Why are gamma oscillations unique among neuronal rhythms in mediating this effect on consolidation? It was theorized that gamma has specific properties that help promote effective interregional communications (Engel et al., 2001; Fries, 2015; Wang, 2010). Their frequency matches the timing of synaptic interactions between principal cells and interneurons, while also creating favorable circumstances for many types of synaptic plasticity (Traub et al., 1998; Wespatat et al. 2004; Zarnadze et al., 2016). Furthermore, they are frequently coupled with slower rhythms such as theta oscillations, which can facilitate the long-range routing of information between brain regions (Buzsaki and Wang, 2012; Jensen and Colgin, 2007).

A question that arises is how can this BLA rhythm affect consolidation occurring elsewhere? As mentioned in Chapter 1, lesion and inactivation studies have shown that BLA activity is important during the early stages of consolidation for emotional experiences. Its recruitment shortly after emotional experiences is thought to facilitate mnemonic processes in regions that support memory storage and retrieval (McGaugh, 2004). Anatomically, the BLA is bidirectionally connected with areas that participate in consolidation, such as the hippocampus and prefrontal cortex (McDonald, 1991; Pitkanen et al., 2000). More recently, it was shown that the BLA exhibits oscillatory interactions with consolidation-related areas during emotional tasks (Bass and Manns, 2015; Likhtik

and Paz, 2015; Popescu et al., 2009; Stujenske et al., 2014). Importantly though, these interactions persist after an emotional experience, with a recent study showing coordinated reactivation of amygdala-hippocampus neuronal ensembles during post-learning SWRs (Girardeau et al., 2017).

Since gamma oscillations could coordinate cortico-hippocampal interactions, the BLA is ideally positioned to facilitate this communication by augmenting the entrainment of both structures to gamma. This also agrees with findings from Chapter 3, showing increased gamma coherence between the BLA and mPFC right after SWRs. Thus, in these experiments, by boosting or disrupting gamma, the BLA's ability to coordinate with the mPFC was enhanced or diminished, respectively. This potentially changes how effectively the mPFC can integrate hippocampal inputs. Since affecting interactions between the hippocampus and mPFC was shown to modulate consolidation strength (Maingret et al., 2016), this path could lead to the observed effects on behavior, where the same subject would show varying performance on different training days based on whether BLA gamma was up- or downregulated after training.

8.6 Conclusion and future directions

Overall, this is the first study that directly links gamma activity to a cognitive process, namely memory consolidation. Given the ubiquitous nature of gamma rhythms,

this is a first step towards dissecting how gamma facilitates neuronal processes and whether it has a causal role in other phenomena. Furthermore, these results emphasize the importance of precisely timed optogenetic modulation, following endogenous activity patterns. Optogenetics are widely used in neuroscience research, but the majority of studies use fixed stimulation patterns that cause widespread unnatural changes in excitability. As closed-loop methods are becoming more popular, tailoring optogenetic modulation to spontaneous activity may lead to better control of neural circuits and to more specific effects on behavior.

Based on the existing literature, I hypothesized that BLA gamma oscillations modulate consolidation strength by affecting cortico-hippocampal interactions. However, in my experiments I modulated gamma levels locally in the BLA by targeting fast-spiking interneurons. Thus, it is unclear how the modulation specifically affected interactions between BLA and mPFC or vHipp. This could be achieved in future experiments by optogenetically targeting projection cells that innervate one structure or the other. That way, we could assess the importance of specific projection cells in local gamma rhythmogenesis as well as coherence between structures. Alternatively, we could track gamma phase in the BLA but instead stimulate local fast-spiking interneurons in either vHipp or mPFC, in or out-of-phase, mimicking a “functional connection/disconnection”. Ultimately, this novel closed-loop method can support a staggering variety of experiments investigating the different roles of oscillatory rhythms. Hopefully, we will soon be able to answer many lingering questions regarding how the brain uses oscillations to support cognitive functions.

List of references

Adhikari, A., Topiwala, M. A., & Gordon, J. A. (2010). Synchronized activity between the ventral hippocampus and the medial prefrontal cortex during anxiety. *Neuron*, *65*(2), 257-269.

Adhikari, A., Topiwala, M. A., & Gordon, J. A. (2011). Single units in the medial prefrontal cortex with anxiety-related firing patterns are preferentially influenced by ventral hippocampal activity. *Neuron*, *71*(5), 898-910.

Alvarez, P., & Squire, L. R. (1994). Memory consolidation and the medial temporal lobe: a simple network model. *Proceedings of the National Academy of Sciences*, *91*(15), 7041-7045.

Amir, A., Headley, D. B., Lee, S. C., Haufler, D., & Pare, D. (2018). Vigilance-associated gamma oscillations coordinate the ensemble activity of basolateral amygdala neurons. *Neuron*, *97*(3), 656-669.

Atallah, B. V., & Scanziani, M. (2009). Instantaneous modulation of gamma oscillation frequency by balancing excitation with inhibition. *Neuron*, *62*(4), 566-577.

Bannerman, D. M., Rawlins, J. N. P., McHugh, S. B., Deacon, R. M. J., Yee, B. K., *et al.* (2004). Regional dissociations within the hippocampus—memory and anxiety. *Neuroscience & Biobehavioral Reviews*, *28*(3), 273-283.

Barsegyan, A., Mirone, G., Ronzoni, G., Guo, C., Song, Q., *et al.* (2019). Glucocorticoid enhancement of recognition memory via basolateral amygdala-driven facilitation of prelimbic cortex interactions. *Proceedings of the National Academy of Sciences*, *116*(14), 7077-7082.

Bass, D. I., & Manns, J. R. (2015). Memory-enhancing amygdala stimulation elicits gamma synchrony in the hippocampus. *Behavioral Neuroscience*, *129*(3), 244-256.

Bast, T., da Silva, B. M., & Morris, R. G. (2005). Distinct contributions of hippocampal NMDA and AMPA receptors to encoding and retrieval of one-trial place memory. *The Journal of Neuroscience*, *25*(25), 5845-5856.

Bauer, E. P., Paz, R., & Paré, D. (2007). Gamma oscillations coordinate amygdalo-rhinal interactions during learning. *The Journal of Neuroscience*, *27*(35), 9369-9379.

Bi, G. Q., & Poo, M. M. (1998). Synaptic modifications in cultured hippocampal neurons: dependence on spike timing, synaptic strength, and postsynaptic cell type. *The Journal of Neuroscience*, *18*(24), 10464-10472.

Bokil, H., Andrews, P., Kulkarni, J. E., Mehta, S., & Mitra, P. P. (2010). Chronux: a platform for analyzing neural signals. *Journal of Neuroscience Methods*, *192*(1), 146-151.

Bontempi, B., Laurent-Demir, C., Destrade, C., & Jaffard, R. (1999). Time-dependent reorganization of brain circuitry underlying long-term memory storage. *Nature*, *400*(6745), 671-675.

Born, J., & Wilhelm, I. (2012). System consolidation of memory during sleep. *Psychological Research, 76*(2), 192-203.

Bragin, A., Jando, G., Nadasdy, Z., Van Landeghem, M., & Buzsáki, G. (1995a). Dentate EEG spikes and associated interneuronal population bursts in the hippocampal hilar region of the rat. *Journal of Neurophysiology*, *73*(4), 1691-1705.

Bragin, A., Jandó, G., Nádasdy, Z., Hetke, J., Wise, K., *et al.* (1995b). Gamma (40-100 Hz) oscillation in the hippocampus of the behaving rat. *The Journal of Neuroscience*, *15*(1), 47-60.

Bucherelli, C., Tassoni, G., & Bureš, J. (1992). Time-dependent disruption of passive avoidance acquisition by post-training intra-amygdala injection of tetrodotoxin in rats. *Neuroscience Letters*, *140*(2), 231-234.

Buehlmann, A., & Deco, G. (2010). Optimal information transfer in the cortex through synchronization. *PLoS Computational Biology*, *6*(9), e1000934.

Burgos-Robles, A., Kimchi, E. Y., Izadmehr, E. M., Porzenheim, M. J., Ramos-Guasp, W. A., *et al.* (2017). Amygdala inputs to prefrontal cortex guide behavior amid conflicting cues of reward and punishment. *Nature Neuroscience*, *20*(6), 824-835.

Buzsáki, G. (1989). Two-stage model of memory trace formation: a role for "noisy" brain states. *Neuroscience*, *31*(3), 551-570.

Buzsáki, G., Horvath, Z., Urioste, R., Hetke, J. & Wise, K. (1992). High-frequency network oscillation in the hippocampus. *Science, 256*(5059), 1025-1027.

Buzsáki, G., & Schomburg, E. W. (2015). What does gamma coherence tell us about inter-regional neural communication? *Nature Neuroscience*, *18*(4), 484-489.

Buzsáki, G., & Wang, X. J. (2012). Mechanisms of gamma oscillations. *Annual Review of Neuroscience*, *35*, 203-225.

Cahill, L. (2000). Neurobiological mechanisms of emotionally influenced, long-term memory. *Progress in Brain Research*, *126*, 29-37.

Cahill, L., & McGaugh, J. L. (1998). Mechanisms of emotional arousal and lasting declarative memory. *Trends in Neurosciences*, *21*(7), 294-299.

Cardin, J. A., Carlén, M., Meletis, K., Knoblich, U., Zhang, F., *et al.* (2009). Driving fast-spiking cells induces gamma rhythm and controls sensory responses. *Nature*, *459*(7247), 663-667.

Carr, M. F., Karlsson, M. P., & Frank, L. M. (2012). Transient slow gamma synchrony underlies hippocampal memory replay. *Neuron*, *75*(4), 700-713.

Chauvette, S., Seigneur, J., & Timofeev, I. (2012). Sleep oscillations in the thalamocortical system induce long-term neuronal plasticity. *Neuron*, *75*(6), 1105-1113.

Christianson, S. Å. (1992). Emotional stress and eyewitness memory: a critical review. *Psychological Bulletin*, *112*(2), 284-309.

Chrobak, J. J., & Buzsáki, G. (1994). Selective activation of deep layer (V-VI) retrohippocampal cortical neurons during hippocampal sharp waves in the behaving rat. *The Journal of Neuroscience*, *14*(10), 6160-6170.

Ciocchi, S., Passecker, J., Malagon-Vina, H., Mikus, N., & Klausberger, T. (2015). Selective information routing by ventral hippocampal CA1 projection neurons. *Science*, *348*(6234), 560-563.

Colgin, L. L., Denninger, T., Fyhn, M., Hafting, T., Bonnevie, T., *et al.* (2009). Frequency of gamma oscillations routes flow of information in the hippocampus. *Nature*, *462*(7271), 353-357.

Colgin, L. L., Kubota, D., Brucher, F. A., Jia, Y., Branyan, E., *et al.* (2004). Spontaneous waves in the dentate gyrus of slices from the ventral hippocampus. *Journal of Neurophysiology*, *92*(6), 3385-3398.

Colgin, L. L. (2011). Oscillations and hippocampal–prefrontal synchrony. *Current Opinion in Neurobiology*, *21*(3), 467-474.

Colgin, L. L. (2015). Theta–gamma coupling in the entorhinal–hippocampal system. *Current Opinion in Neurobiology*, *31*, 45-50.

Collins, D. R., Pelletier, J. G., & Paré, D. (2001). Slow and fast (gamma) neuronal oscillations in the perirhinal cortex and lateral amygdala. *Journal of Neurophysiology*, *85*(4), 1661-1672.

Courtin, J., Karalis, N., Gonzalez-Campo, C., Wurtz, H., & Herry, C. (2014). Persistence of amygdala gamma oscillations during extinction learning predicts spontaneous fear recovery. *Neurobiology of Learning and Memory*, *113*, 82-89.

Csicsvari, J., Hirase, H., Mamiya, A., & Buzsáki, G. (2000). Ensemble patterns of hippocampal CA3-CA1 neurons during sharp wave–associated population events. *Neuron*, *28*(2), 585-594.

Davis, P., Zaki, Y., Maguire, J., & Reijmers, L. G. (2017). Cellular and oscillatory substrates of fear extinction learning. *Nature Neuroscience*, *20*(11), 1624-1633.

Dejean, C., Courtin, J., Karalis, N., Chaudun, F., Wurtz, H., Bienvenu, T. C., & Herry, C. (2016). Prefrontal neuronal assemblies temporally control fear behaviour. *Nature*, *535*(7612), 420-424.

Drieu, C., Todorova, R., & Zugaro, M. (2018). Nested sequences of hippocampal assemblies during behavior support subsequent sleep replay. *Science*, *362*(6415), 675-679.

Ego-Stengel, V., & Wilson, M. A. (2010). Disruption of ripple-associated hippocampal activity during rest impairs spatial learning in the rat. *Hippocampus*, *20*(1), 1-10.

Engel, A. K., Fries, P., & Singer, W. (2001). Dynamic predictions: oscillations and synchrony in top–down processing. *Nature Reviews Neuroscience*, *2*(10), 704-716.

Eschenko, O., Ramadan, W., Mölle, M., Born, J., & Sara, S. J. (2008). Sustained increase in hippocampal sharp-wave ripple activity during slow-wave sleep after learning. *Learning & Memory*, *15*(4), 222-228.

Fanselow, M. S., & Dong, H. W. (2010). Are the dorsal and ventral hippocampus functionally distinct structures? *Neuron*, *65*(1), 7-19.

Felix-Ortiz, A. C., Beyeler, A., Seo, C., Leppla, C. A., Wildes, C. P., *et al.* (2013). BLA to vHPC inputs modulate anxiety-related behaviors. *Neuron*, *79*(4), 658-664.

Felix-Ortiz, A. C., Burgos-Robles, A., Bhagat, N. D., Leppla, C. A., & Tye, K. M. (2016). Bidirectional modulation of anxiety-related and social behaviors by amygdala projections to the medial prefrontal cortex. *Neuroscience*, *321*, 197-209.

Felix-Ortiz, A. C., & Tye, K. M. (2014). Amygdala inputs to the ventral hippocampus bidirectionally modulate social behavior. *The Journal of Neuroscience*, *34*(2), 586-595.

Fell, J., Klaver, P., Lehnertz, K., Grunwald, T., Schaller, C., *et al.* (2001). Human memory formation is accompanied by rhinal–hippocampal coupling and decoupling. *Nature Neuroscience*, *4*(12), 1259-1264.

Feng, F., Headley, D. B., Amir, A., Kanta, V., Chen, Z., Paré, D., & Nair, S. (2019). Gamma oscillations in the basolateral amygdala: biophysical mechanisms and computational consequences. *eNeuro*, 0388.

Fernández-Ruiz, A., Muñoz, S., Sancho, M., Makarova, J., Makarov, V. A., *et al.* (2013). Cytoarchitectonic and dynamic origins of giant positive local field potentials in the dentate gyrus. *The Journal of Neuroscience*, *33*(39), 15518-15532.

Floresco, S. B., Seamans, J. K., & Phillips, A. G. (1997). Selective roles for hippocampal, prefrontal cortical, and ventral striatal circuits in radial-arm maze tasks with or without a delay. *The Journal of Neuroscience*, *17*(5), 1880-1890.

Floresco, S. B., & Tse, M. T. (2007). Dopaminergic regulation of inhibitory and excitatory transmission in the basolateral amygdala–prefrontal cortical pathway. *The Journal of Neuroscience*, *27*(8), 2045-2057.

Frankland, P. W., & Bontempi, B. (2005). The organization of recent and remote memories. *Nature Reviews Neuroscience*, *6*(2), 119.

Fries, P. (2005). A mechanism for cognitive dynamics: neuronal communication through neuronal coherence. *Trends in Cognitive Sciences*, *9*(10), 474-480.

Fries, P. (2015). Rhythms for cognition: communication through coherence. *Neuron*, *88*(1), 220-235.

Gale, G. D., Anagnostaras, S. G., Godsil, B. P., Mitchell, S., Nozawa, T., *et al.* (2004). Role of the basolateral amygdala in the storage of fear memories across the adult lifetime of rats. *The Journal of Neuroscience*, *24*(15), 3810-3815.

Gallagher, M., & Kapp, B. S. (1981). Effect of phentolamine administration into the amygdala complex of rats on time-dependent memory processes. *Behavioral and Neural Biology*, *31*(1), 90-95.

Gallagher, M., Kapp, B. S., Musty, R. E., & Driscoll, P. A. (1977). Memory formation: evidence for a specific neurochemical system in the amygdala. *Science*, *198*(4315), 423-425.

Girardeau, G., Benchenane, K., Wiener, S. I., Buzsáki, G., & Zugaro, M. B. (2009). Selective suppression of hippocampal ripples impairs spatial memory. *Nature Neuroscience*, *12*(10), 1222-1223.

Girardeau, G., Inema, I., & Buzsáki, G. (2017). Reactivations of emotional memory in the hippocampus–amygdala system during sleep. *Nature Neuroscience*, *20*(11), 1634-1642.

Goddard, G. V. (1964). Amygdaloid stimulation and learning in the rat. *Journal of Comparative and Physiological Psychology*, *58*(1), 23-30.

Gold, P. E., Hankins, L., Edwards, R. M., Chester, J., & McGaugh, J. L. (1975). Memory interference and facilitation with posttrial amygdala stimulation: Effect on memory varies with footshock level. *Brain Research*, *86*(3), 509-513.

Gold, P. E., & McGaugh, J. L. (1975). A single-trace, two-process view of memory storage processes. (Deutsch, J. and Deutsch, D., eds) *Short-Term Memory*, 355-378. Academic Press.

Gründemann, J., & Lüthi, A. (2015). Ensemble coding in amygdala circuits for associative learning. *Current Opinion in Neurobiology*, *35*, 200-206.

Haider, B., Duque, A., Hasenstaub, A. R., & McCormick, D. A. (2006). Neocortical network activity in vivo is generated through a dynamic balance of excitation and inhibition. *The Journal of Neuroscience*, *26*(17), 4535-4545.

Harris, K. D., Henze, D. A., Csicsvari, J., Hirase, H., & Buzsaki, G. (2000). Accuracy of tetrode spike separation as determined by simultaneous intracellular and extracellular measurements. *Journal of Neurophysiology, 84*(1), 401-414.

Hasenstaub, A., Shu, Y., Haider, B., Kraushaar, U., Duque, A., & McCormick, D. A. (2005). Inhibitory postsynaptic potentials carry synchronized frequency information in active cortical networks. *Neuron, 47*(3), 423-435.

Hazan, L., Zugaro, M., & Buzsáki, G. (2006). Klusters, NeuroScope, NDManager: a free software suite for neurophysiological data processing and visualization. *Journal of Neuroscience Methods*, *155*(2), 207-216.

Headley, D. B., Kanta, V., & Pare, D. (2016). Intra-and inter-regional cortical interactions related to sharp wave ripples and dentate spikes. *Journal of Neurophysiology*, jn-00644.

Headley, D. B., DeLucca, M. V., Haufler, D., & Paré, D. (2015). Incorporating 3D-printing technology in the design of head-caps and electrode drives for recording neurons in multiple brain regions. *Journal of Neurophysiology*, *113*(7), 2721-2732.

Headley, D. B., & Paré, D. (2013). In sync: gamma oscillations and emotional memory. *Frontiers in Behavioral Neuroscience*, *7*: 170.

Headley, D. B., & Weinberger, N. M. (2011). Gamma-band activation predicts both associative memory and cortical plasticity. *The Journal of Neuroscience*, *31*(36), 12748-12758.

Huff, M. L., Emmons, E. B., Narayanan, N. S., & LaLumiere, R. T. (2016). Basolateral amygdala projections to ventral hippocampus modulate the consolidation of footshock, but not contextual, learning in rats. *Learning & Memory*, *23*(2), 51-60.

Huff, M. L., Miller, R. L., Deisseroth, K., Moorman, D. E., & LaLumiere, R. T. (2013). Posttraining optogenetic manipulations of basolateral amygdala activity modulate consolidation of inhibitory avoidance memory in rats. *Proceedings of the National Academy of Sciences*, *110*(9), 3597-3602.

Inman, C. S., Manns, J. R., Bijanki, K. R., Bass, D. I., Hamann, S., Drane, D. L., Fasano, R.E., Kovach, C.K., Gross, R.E., & Willie, J. T. (2018). Direct electrical stimulation of the amygdala enhances declarative memory in humans. *Proceedings of the National Academy of Sciences*, *115*(1), 98-103.

Jadhav, S. P., Kemere, C., German, P. W., & Frank, L. M. (2012). Awake hippocampal sharp-wave ripples support spatial memory. *Science*, *336*(6087), 1454-1458.

Jadhav, S. P., Rothschild, G., Roumis, D. K., & Frank, L. M. (2016). Coordinated excitation and inhibition of prefrontal ensembles during awake hippocampal sharp-wave ripple events. *Neuron*, *90*(1), 113-127.

Jazayeri, M., & Afraz, A. (2017). Navigating the neural space in search of the neural code. *Neuron*, *93*(5), 1003-1014.

Jensen, O., & Colgin, L. L. (2007). Cross-frequency coupling between neuronal oscillations. *Trends in Cognitive Sciences*, *11*(7), 267-269.

Ji, D., & Wilson, M. A. (2007). Coordinated memory replay in the visual cortex and hippocampus during sleep. *Nature Neuroscience*, *10*(1), 100-107.

Jutras, M. J., Fries, P., & Buffalo, E. A. (2009). Gamma-band synchronization in the macaque hippocampus and memory formation. *The Journal of Neuroscience*, *29*(40), 12521-12531.

Khodagholy, D., Gelinas, J. N., & Buzsáki, G. (2017). Learning-enhanced coupling between ripple oscillations in association cortices and hippocampus. *Science*, *358*(6361), 369-372.

Klapoetke, N. C., Murata, Y., Kim, S. S., Pulver, S. R., Birdsey-Benson, A., *et al.* (2014). Independent optical excitation of distinct neural populations. *Nature Methods*, *11*(3), 338-346.

Klavir, O., Prigge, M., Sarel, A., Paz, R., & Yizhar, O. (2017). Manipulating fear associations via optogenetic modulation of amygdala inputs to prefrontal cortex. *Nature Neuroscience*, *20*(6), 836.

Kudrimoti, H. S., Barnes, C. A., & McNaughton, B. L. (1999). Reactivation of hippocampal cell assemblies: effects of behavioral state, experience, and EEG dynamics. *The Journal of Neuroscience*, *19*(10), 4090-4101.

LeDoux, J. (2003). The emotional brain, fear, and the amygdala. *Cellular and Molecular Neurobiology*, *23*(4-5), 727-738.

Lensu, S., Waselius, T., Penttonen, M., & Nokia, M. S. (2019). Dentate spikes and learning: disrupting hippocampal function during memory consolidation can improve pattern separation. *Journal of Neurophysiology*, 121(1), 131-139.

Łęski, S., Pettersen, K. H., Tunstall, B., Einevoll, G. T., Gigg, J., & Wójcik, D. K. (2011). Inverse current source density method in two dimensions: inferring neural activation from multielectrode recordings. Neuroinformatics, *9*(4), 401-425.

Liang, K. C., McGaugh, J. L., Martinez, J. L., Jensen, R. A., Vasquez, B. J., *et al.* (1982). Post-training amygdaloid lesions impair retention of an inhibitory avoidance response. *Behavioural Brain Research*, *4*(3), 237-249.

Likhtik, E., & Paz, R. (2015). Amygdala–prefrontal interactions in (mal) adaptive learning. *Trends in Neurosciences*, *38*(3), 158-166.

Likhtik, E., Pelletier, J. G., Paz, R., & Paré, D. (2005). Prefrontal control of the amygdala. *The Journal of Neuroscience*, *25*(32), 7429-7437.

Likhtik, E., Stujenske, J. M., Topiwala, M. A., Harris, A. Z., & Gordon, J. A. (2014). Prefrontal entrainment of amygdala activity signals safety in learned fear and innate anxiety. *Nature Neuroscience*, *17*(1), 106-113.

Lundqvist, M., Rose, J., Herman, P., Brincat, S. L., Buschman, T. J., & Miller, E. K. (2016). Gamma and beta bursts underlie working memory. *Neuron*, *90*(1), 152-164.

Malvache, A., Reichinnek, S., Villette, V., Haimerl, C., & Cossart, R. (2016). Awake hippocampal reactivations project onto orthogonal neuronal assemblies. *Science, 353*(6305), 1280-1283.

Maren, S., & Fanselow, M. S. (1995). Synaptic plasticity in the basolateral amygdala induced by hippocampal formation stimulation in vivo. *The Journal of Neuroscience*, *15*(11), 7548-7564.

Markram, H., Lübke, J., Frotscher, M., & Sakmann, B. (1997). Regulation of synaptic efficacy by coincidence of postsynaptic APs and EPSPs. *Science*, *275*(5297), 213-215.

Marr, D. (1970). A theory for cerebral neocortex. *Proceedings of the Royal Society of London, 176*, 161-234.

Maingret, N., Girardeau, G., Todorova, R., Goutierre, M., & Zugaro, M. (2016). Hippocampo-cortical coupling mediates memory consolidation during sleep. *Nature Neuroscience*, *19*(7), 959-964.

Marek, R., Jin, J., Goode, T. D., Giustino, T. F., Wang, Q., *et al.* (2018). Hippocampus-driven feed-forward inhibition of the prefrontal cortex mediates relapse of extinguished fear. *Nature Neuroscience, 21*(3), 384-392.

Marshall, L., Helgadóttir, H., Mölle, M., & Born, J. (2006). Boosting slow oscillations during sleep potentiates memory. *Nature*, *444*(7119), 610-613.

Maviel, T., Durkin, T. P., Menzaghi, F., & Bontempi, B. (2004). Sites of neocortical reorganization critical for remote spatial memory. *Science, 305*(5680), 96-99.

McDonald, A. J. (1991). Organization of amygdaloid projections to the prefrontal cortex and associated striatum in the rat. *Neuroscience*, *44*(1), 1-14.

McDonald, A. J. (1998). Cortical pathways to the mammalian amygdala. *Progress in Neurobiology*, *55*(3), 257-332.

McGaugh, J. L. (2004). The amygdala modulates the consolidation of memories of emotionally arousing experiences. *Annual Review of Neuroscience, 27*, 1-28.

McGarry, L. M., & Carter, A. G. (2016). Inhibitory Gating of Basolateral Amygdala Inputs to the Prefrontal Cortex. *The Journal of Neuroscience, 36*(36), 9391-9406.

McReynolds, J. R., Anderson, K. M., Donowho, K. M., & McIntyre, C. K. (2014). Noradrenergic actions in the basolateral complex of the amygdala modulate Arc expression in hippocampal synapses and consolidation of aversive and non-aversive memory. *Neurobiology of Learning and Memory, 115*, 49-57.

Miltner, W. H., Braun, C., Arnold, M., Witte, H., & Taub, E. (1999). Coherence of gamma-band EEG activity as a basis for associative learning. *Nature*, *397*(6718), 434-436.

Miyamoto, D., Hirai, D., Fung, C. C. A., Inutsuka, A., Odagawa, M., *et al.* (2016). Top-down cortical input during NREM sleep consolidates perceptual memory. *Science*, *352*(6291), 1315-1318.

Mölle, M., Marshall, L., Gais, S., & Born, J. (2004). Learning increases human electroencephalographic coherence during subsequent slow sleep oscillations. *Proceedings of the National Academy of Sciences of the United States of America*, *101*(38), 13963-13968.

Mölle, M., Yeshenko, O., Marshall, L., Sara, S. J., & Born, J. (2006). Hippocampal sharp wave-ripples linked to slow oscillations in rat slow-wave sleep. *Journal of Neurophysiology*, *96*(1), 62-70.

Morris, R. G. M. (1991). Distinctive computations and relevant associative processes: Hippocampal role in processing, retrieval, but not storage of allocentric spatial memory. *Hippocampus*, *1*(3), 287-290.

Müller, G. E., & Pilzecker, A. (1900). Experimentelle beiträge zur lehre vom gedächtnis. *Z. Psychol.* (Suppl. 1).

Nádasdy, Z., Hirase, H., Czurkó, A., Csicsvari, J., & Buzsáki, G. (1999). Replay and time compression of recurring spike sequences in the hippocampus. *The Journal of Neuroscience*, *19*(21), 9497-9507.

Narayanan, R. T., Seidenbecher, T., Kluge, C., Bergado, J., Stork, O., *et al.* (2007). Dissociated theta phase synchronization in amygdalo-hippocampal circuits during various stages of fear memory. *European Journal of Neuroscience*, *25*(6), 1823-1831.

Nathanson, J. L., Yanagawa, Y., Obata, K., & Callaway, E. M. (2009). Preferential labeling of inhibitory and excitatory cortical neurons by endogenous tropism of adeno-associated virus and lentivirus vectors. *Neuroscience*, *161*(2), 441-450.

Ngo, H. V. V., Martinetz, T., Born, J., & Mölle, M. (2013). Auditory closed-loop stimulation of the sleep slow oscillation enhances memory. *Neuron*, *78*(3), 545-553.

Ni, J., Wunderle, T., Lewis, C. M., Desimone, R., Diester, I., *et al.* (2016). Gamma-rhythmic gain modulation. *Neuron*, *92*(1), 240-251.

Nicholson, E., Kuzmin, D. A., Leite, M., Akam, T. E., & Kullmann, D. M. (2018). Analogue closed-loop optogenetic modulation of hippocampal pyramidal cells dissociates gamma frequency and amplitude. *eLife*, *7*, e38346.

Nokia, M. S., Penttonen, M., & Wikgren, J. (2010). Hippocampal ripple-contingent training accelerates trace eyeblink conditioning and retards extinction in rabbits. *The Journal of Neuroscience*, *30*(34), 11486-11492.

Nokia, M. S., Gureviciene, I., Waselius, T., Tanila, H., & Penttonen, M. (2017). Hippocampal electrical stimulation disrupts associative learning when targeted at dentate spikes. *The Journal of Physiology*, *595*(14), 4961-4971.

Norimoto, H., Makino, K., Gao, M., Shikano, Y., Okamoto, K., Ishikawa, T., Sasaki, T., Hioki, H., Fujisawa, S., & Ikegaya, Y. (2018). Hippocampal ripples down-regulate synapses. *Science*, *359*(6383), 1524-1527.

O'Keefe, J. (1979). A review of the hippocampal place cells. *Progress in neurobiology*, *13*(4), 419-439.

Ólafsdóttir, H. F., Carpenter, F., & Barry, C. (2016). Coordinated grid and place cell replay during rest. *Nature Neuroscience*, *19*(6), 792-794.

Orsini, C. A., Kim, J. H., Knapska, E., & Maren, S. (2011). Hippocampal and prefrontal projections to the basal amygdala mediate contextual regulation of fear after extinction. *The Journal of Neuroscience*, *31*(47), 17269-17277.

Packard, M. G., Cahill, L., & McGaugh, J. L. (1994). Amygdala modulation of hippocampal-dependent and caudate nucleus-dependent memory processes. *Proceedings of the National Academy of Sciences*, *91*(18), 8477-8481.

Packard, M. G., & Teather, L. A. (1998). Amygdala modulation of multiple memory systems: hippocampus and caudate-putamen. *Neurobiology of Learning and Memory*, *69*(2), 163-203.

Padilla-Coreano, N., Bolkan, S. S., Pierce, G. M., Blackman, D. R., Hardin, W. D., *et al.* (2016). Direct ventral hippocampal-prefrontal input is required for anxiety-related neural activity and behavior. *Neuron*, *89*(4), 857-866.

Palmigiano, A., Geisel, T., Wolf, F., & Battaglia, D. (2017). Flexible information routing by transient synchrony. *Nature Neuroscience*, *20*(7), 1014.

Paré, D., Dong, J., & Gaudreau, H. (1995). Amygdalo-entorhinal relations and their reflection in the hippocampal formation: generation of sharp sleep potentials. *The Journal of Neuroscience*, *15*(3), 2482-2503.

Paré, D., & Gaudreau, H. (1996). Projection cells and interneurons of the lateral and basolateral amygdala: distinct firing patterns and differential relation to theta and delta rhythms in conscious cats. *The Journal of Neuroscience*, *16*(10), 3334-3350.

Pavlides, C., & Winson, J. (1989). Influences of hippocampal place cell firing in the awake state on the activity of these cells during subsequent sleep episodes. *The Journal of Neuroscience*, *9*(8), 2907-2918.

Penttonen, M., Kamondi, A., Sik, A., Acsády, L., & Buzsáki, G. (1997). Feed-forward and feed-back activation of the dentate gyrus in vivo during dentate spikes and sharp wave bursts. *Hippocampus*, *7*(4), 437-450.

Penttonen, M., Kamondi, A., Acsády, L., & Buzsáki, G. (1998). Gamma frequency oscillation in the hippocampus of the rat: intracellular analysis in vivo. *European Journal of Neuroscience*, *10*(2), 718-728.

Peyrache, A., Khamassi, M., Benchenane, K., Wiener, S. I., & Battaglia, F. P. (2009). Replay of rule-learning related neural patterns in the prefrontal cortex during sleep. *Nature Neuroscience*, *12*(7), 919-926.

Pitkänen, A., Pikkarainen, M., Nurminen, N., & Ylinen, A. (2000). Reciprocal connections between the amygdala and the hippocampal formation, perirhinal cortex, and postrhinal cortex in rat: a review. *Annals of the New York Academy of Sciences*, *911*(1), 369-391.

Popescu, A. T., Popa, D., & Paré, D. (2009). Coherent gamma oscillations couple the amygdala and striatum during learning. *Nature Neuroscience*, *12*(6), 801-807.

Qin, Y. L., Mcnaughton, B. L., Skaggs, W. E., & Barnes, C. A. (1997). Memory reprocessing in corticocortical and hippocampocortical neuronal ensembles. *Philosophical Transactions of the Royal Society of London B: Biological Sciences*, *352*(1360), 1525-1533.

Ramadan, W., Eschenko, O., & Sara, S. J. (2009). Hippocampal sharp wave/ripples during sleep for consolidation of associative memory. *PloS One*, *4*(8), e6697.

Remondes, M., & Wilson, M. A. (2015). Slow-γ Rhythms Coordinate Cingulate Cortical Responses to Hippocampal Sharp-Wave Ripples during Wakefulness. *Cell Reports*, *13*(7), 1327-1335.

Rohenkohl, G., Bosman, C. A., & Fries, P. (2018). Gamma synchronization between V1 and V4 improves behavioral performance. *Neuron*, *100*(4), 953-963.

Roozendaal, B., & McGaugh, J. L. (1997). Glucocorticoid receptor agonist and antagonist administration into the basolateral but not central amygdala modulates memory storage. *Neurobiology of Learning and Memory*, *67*(2), 176-179.

Roozendaal, B., McReynolds, J. R., Van der Zee, E. A., Lee, S., McGaugh, J. L., *et al.* (2009). Glucocorticoid effects on memory consolidation depend on functional interactions between the medial prefrontal cortex and basolateral amygdala. *The Journal of Neuroscience*, *29*(45), 14299-14308.

Rosenkranz, J. A., & Grace, A. A. (2001). Dopamine attenuates prefrontal cortical suppression of sensory inputs to the basolateral amygdala of rats. *The Journal of Neuroscience*, *21*(11), 4090-4103.

Rothschild, G., Eban, E., & Frank, L.M. (2017). A cortical–hippocampal–cortical loop of information processing during memory consolidation. *Nature Neuroscience*, *20*(2), 251-259.

Roux, L., Hu, B., Eichler, R., Stark, E., & Buzsáki, G. (2017). Sharp wave ripples during learning stabilize the hippocampal spatial map. *Nature Neuroscience*, *20*(6), 845-853.

Sadowski, J. H., Jones, M. W., & Mellor, J. R. (2016). Sharp-Wave Ripples Orchestrate the Induction of Synaptic Plasticity during Reactivation of Place Cell Firing Patterns in the Hippocampus. *Cell Reports*, *14*(8), 1916-1929.

Sasaki, T., Piatti, V. C., Hwaun, E., Ahmadi, S., Lisman, J. E., *et al.* (2018). Dentate network activity is necessary for spatial working memory by supporting CA3 sharp-wave ripple generation and prospective firing of CA3 neurons. *Nature Neuroscience*, *21*(2), 258-269.

Sato, W., Kochiyama, T., Uono, S., Matsuda, K., Usui, K., *et al.* (2011). Rapid amygdala gamma oscillations in response to fearful facial expressions. *Neuropsychologia*, *49*(4), 612-617.

Schomburg, E. W., Fernández-Ruiz, A., Mizuseki, K., Berényi, A., Anastassiou, C. A., *et al.* (2014). Theta phase segregation of input-specific gamma patterns in entorhinal-hippocampal networks. *Neuron*, *84*(2), 470-485.

Scoville, W. B., & Milner, B. (1957). Loss of recent memory after bilateral hippocampal lesions. *Journal of Neurology, Neurosurgery & Psychiatry*, *20*(1), 11-21.

Sederberg, P. B., Schulze-Bonhage, A., Madsen, J. R., Bromfield, E. B., McCarthy, D. C., *et al.* (2007). Hippocampal and neocortical gamma oscillations predict memory formation in humans. *Cerebral Cortex*, *17*(5), 1190-1196.

Seidenbecher, T., Laxmi, T. R., Stork, O., & Pape, H. C. (2003). Amygdalar and hippocampal theta rhythm synchronization during fear memory retrieval. *Science*, *301*(5634), 846-850.

Shu, Y., Hasenstaub, A., & McCormick, D. A. (2003). Turning on and off recurrent balanced cortical activity. *Nature*, *423*(6937), 288-293.

Siegel, M., Warden, M. R., & Miller, E. K. (2009). Phase-dependent neuronal coding of objects in short-term memory. *Proceedings of the National Academy of Sciences*, *106*(50), 21341-21346.

Siegle, J. H., Pritchett, D. L., & Moore, C. I. (2014). Gamma-range synchronization of fast-spiking interneurons can enhance detection of tactile stimuli. *Nature Nneuroscience*, *17*(10), 1371-1379.

Siegle, J. H., & Wilson, M. A. (2014). Enhancement of encoding and retrieval functions through theta phase-specific manipulation of hippocampus. *eLife*, *3*, e03061.

Sirota, A., Csicsvari, J., Buhl, D., & Buzsáki, G. (2003). Communication between neocortex and hippocampus during sleep in rodents. *Proceedings of the National Academy of Sciences*, *100*(4), 2065-2069.

Skaggs, W. E., & McNaughton, B. L. (1996). Theta phase precession in hippocampal. *Hippocampus*, *6*, 149-172.

Sohal, V. S., Zhang, F., Yizhar, O., & Deisseroth, K. (2009). Parvalbumin neurons and gamma rhythms enhance cortical circuit performance. *Nature*, *459*(7247), 698-702.

Sotres-Bayon, F., Sierra-Mercado, D., Pardilla-Delgado, E., & Quirk, G. J. (2012). Gating of fear in prelimbic cortex by hippocampal and amygdala inputs. *Neuron*, *76*(4), 804-812.

Squire, L. R., & Alvarez, P. (1995). Retrograde amnesia and memory consolidation: a neurobiological perspective. *Current Opinion in Neurobiology*, *5*(2), 169-177.

Squire, L. R. (1986). Mechanisms of memory. *Science*, *232*(4758), 1612-1619.

Stujenske, J. M., Likhtik, E., Topiwala, M. A., & Gordon, J. A. (2014). Fear and safety engage competing patterns of theta-gamma coupling in the basolateral amygdala. *Neuron*, *83*(4), 919-933.

Stujenske, J. M., Spellman, T., & Gordon, J. A. (2015). Modeling the spatiotemporal dynamics of light and heat propagation for in vivo optogenetics. *Cell Reports*, *12*(3), 525-534.

Sutherland, G. R., & McNaughton, B. (2000). Memory trace reactivation in hippocampal and neocortical neuronal ensembles. *Current Opinion in Neurobiology*, *10*(2), 180-186.

Tallon-Baudry, C., & Bertrand, O. (1999). Oscillatory gamma activity in humans and its role in object representation. *Trends in Cognitive Sciences*, *3*(4), 151-162.

Taub, A. H., Perets, R., Kahana, E., & Paz, R. (2018). Oscillations synchronize amygdala-to-prefrontal primate circuits during aversive learning. *Neuron*, *97*(2), 291-298.

Todorova, R., & Zugaro, M. (2018). Hippocampal ripples as a mode of communication with cortical and subcortical areas. *Hippocampus*, 1-11.

Traub, R. D., Bibbig, A., LeBeau, F. E., Buhl, E. H., & Whittington, M. A. (2004). Cellular mechanisms of neuronal population oscillations in the hippocampus in vitro. *Annual Review of Neuroscience*, *27*, 247-278.

Traub, R. D., Spruston, N., Soltesz, I., Konnerth, A., Whittington, M. A., *et al.* (1998). Gamma-frequency oscillations: a neuronal population phenomenon, regulated by synaptic and intrinsic cellular processes, and inducing synaptic plasticity. *Progress in Neurobiology*, *55*(6), 563-575.

Traub, R. D., Whittington, M. A., Colling, S. B., Buzsáki, G., & Jefferys, J. G. (1996). Analysis of gamma rhythms in the rat hippocampus in vitro and in vivo. *The Journal of Physiology*, *493*(2), 471.

Trimper, J. B., Galloway, C. R., Jones, A. C., Mandi, K., & Manns, J. R. (2017). Gamma oscillations in rat hippocampal subregions dentate gyrus, CA3, CA1, and subiculum underlie associative memory encoding. *Cell Reports, 21*(9), 2419-2432.

Vinck, M., van Wingerden, M., Womelsdorf, T., Fries, P., & Pennartz, C. M. (2010). The pairwise phase consistency: a bias-free measure of rhythmic neuronal synchronization. *Neuroimage, 51*(1), 112-122.

Wang, X. J., & Buzsáki, G. (1996). Gamma oscillation by synaptic inhibition in a hippocampal interneuronal network model. *The Journal of Neuroscience, 16*(20), 6402-6413.

Wang, X. J. (2010). Neurophysiological and computational principles of cortical rhythms in cognition. *Physiological Reviews, 90*(3), 1195-1268.

Wang, G. W., & Cai, J. X. (2006). Disconnection of the hippocampal–prefrontal cortical circuits impairs spatial working memory performance in rats. *Behavioural Brain Research*, *175*(2), 329-336.

Wang, S. H., & Morris, R. G. (2010). Hippocampal-neocortical interactions in memory formation, consolidation, and reconsolidation. *Annual Review of Psychology*, *61*, 49-79.

Wespatat, V., Tennigkeit, F., & Singer, W. (2004). Phase sensitivity of synaptic modifications in oscillating cells of rat visual cortex. *The Journal of Neuroscience*, *24*(41), 9067-9075.

Whittington, M. A., Cunningham, M. O., LeBeau, F. E., Racca, C., & Traub, R. D. (2011). Multiple origins of the cortical gamma rhythm. *Developmental Neurobiology*, *71*(1), 92-106.

Wilson, M. A., & McNaughton, B. L. (1994). Reactivation of hippocampal ensemble memories during sleep. *Science, 265*(5172), 676-679.

Wiltgen, B. J., Brown, R. A., Talton, L. E., & Silva, A. J. (2004). New circuits for old memories: the role of the neocortex in consolidation. *Neuron*, *44*(1), 101-108.

Wu, C. T., Haggerty, D., Kemere, C., & Ji, D. (2017). Hippocampal awake replay in fear memory retrieval. *Nature Neuroscience, 20*(4), 571-580.

Ylinen, A., Bragin, A., Nádasdy, Z., Jandó, G., Szabo, I., *et al.* (1995). Sharp wave-associated high-frequency oscillation (200 Hz) in the intact hippocampus: network and intracellular mechanisms. *The Journal of Neuroscience*, *15*(1), 30-46.

Zanatta, M. S., Quillfeldt, J. H., Schaeffer, E., Schmitz, P. K., Quevedo, J., *et al.* (1997). Involvement of the hippocampus, amygdala, entorhinal cortex and posterior parietal cortex in memory consolidation. *Brazilian Journal of Medical and Biological Research*, *30*, 235-240.

Zarnadze, S., Bäuerle, P., Santos-Torres, J., Böhm, C., Schmitz, D., *et al.* (2016). Cell-specific synaptic plasticity induced by network oscillations. *eLife, 5*, e14912.

Zheng, C., Bieri, K. W., Hsiao, Y. T., & Colgin, L. L. (2016). Spatial sequence coding differs during slow and fast gamma rhythms in the hippocampus. *Neuron, 89*(2), 398-408.

Zheng, J., Anderson, K. L., Leal, S. L., Shestyuk, A., Gulsen, G., *et al.* (2017). Amygdala-hippocampal dynamics during salient information processing. *Nature Communications, 8*, 14413.